Electrokinetic Processes for Microfluidic Devices

by

Jeffrey Thomas Coleman
B.Sc. Queen's University, 2003

A Thesis Submitted in Partial Fulfillment of the
Requirements for the Degree of

MASTER OF APPLIED SCIENCE

in the Department of Mechanical Engineering

Supervisor: Dr. David Sinton
Department of Mechanical Engineering

ABSTRACT

This thesis is devoted to the development of electrokinetic process for use with microfluidic devices. The study is limited to low Reynolds number, electrokinetic liquid flows in microchannels with hydraulic diameters ranging from 25μm to 200μm. These parameters are typical of the targeted applications of interest, analytical microfluidic chips. A microfluidic mixing strategy was developed which exploits stream-wise diffusion of a sequentially interlaced fluid stream. A numerical model is developed, implemented and applied to demonstrate the microfluidic mixing technique and predict its performance. Based on the numerical results, prototype microfluidic chips are fabricated using soft-lithography methods. Fluorescence microscopy is employed to analyze, quantify and demonstrate the effectiveness of this mixing strategy, as well as to determine an optimal frequency range for operation. A novel strategy for three-dimensional hydrodynamic focusing in a planar microfluidic geometry is developed and tested numerically. Both the microfluidic mixing and focusing technologies developed here have unique advantages over current methods.

TABLE OF CONTENTS

LIST OF FIGURES

LIST OF TABLES

ACKNOWLEDGEMENTS

I would like to express my deepest gratitude to my supervisor, Dr. David Sinton, for his excellent guidance, support, patience, and providing me with an excellent atmosphere for doing research. His enthusiasm and motivation encouraged me to learn and to grow as an individual. I thank Dr. Sinton for giving me the opportunity to work with him.

I would like to thank the members of the Microfluidics Lab for all of the insight, feedback and laughs that will make this experience so memorable. A special thanks to the many friends that I have met while living in Victoria. In particular, I would like to thank Kim Collopy for supporting me through good times and bad.

This research was made possible through financial support provided by the Natural Science and Engineering Research Council of Canada (NSERC) and the Advanced Systems Institute of British Columbia (BCIC). I would also like to acknowledge Dr. Pollard from Queen's University for encouraging me to pursue my Masters degree.

Finally, it is to my family that I dedicate this work. The loving support and encouragement from Ennis, Hugh and Jocelyn was truly incredible. Thank-you.

Chapter 1

INTRODUCTION

1.1 Aims and Motivations of the Thesis

In this thesis, electrokinetic processes have been developed and investigated, namely a microfluidic mixer and a three-dimensional microfluidic focuser. Both numerical and experimental investigations have been performed in order to validate these developments. Due to the dependence of geometry and flow rate when studying fluid interactions, the studies have been limited to the case of microchannels with hydraulic diameters on the order of 100μm and Reynolds numbers in the range of unity. The main goals of this work are: the development and testing of the sequential sample micromixing concept; the development of an operating sequential sample injection scheme; the application of this method to obtain rapid and complete mixing with variable outlet concentration; and the development of a strategy for three-dimensional hydrodynamic focusing on-chip.

The field of microfluidics has grown tremendously over the past 10 years due primarily to growing interest in microfluidic-chip based analytical and diagnostic

applications. The progression of developments in microfluidic engineering is documented in review papers spanning several years [Brody et al. (1996), Bousse et al. (2000), Stone and Kim (2001), Whitesides and Stroock (2001), Stone et al. (2004)], book chapters [Sharp et al. (2002)], and recent books [Nguyen and Wereley (2002), Breuer (2004), Li (2004)]. Microfluidic chip-based technologies can offer many advantages over their traditional macro-sized counterparts. Most notably, microfluidic chip networks benefit from the increase in surface area to volume ratio which accompanies miniaturization. This translates into reduced sample requirements, improved heat dissipation and faster processing. In addition, there is a dramatic reduction in the length scales associated with fluid flow. The result is a sharp increase in surface to volume ratio, leading to an increased influence of surface effects. Furthermore, typical flow parameters are significantly different than their macroscale counterparts. Consider the Reynolds number, which is a dimensionless parameter relating the relative contribution of inertial and viscous effects. For a 1cm diameter pipe, with water flowing at 10cm/s (10 diameters per second), the Reynolds number has a value of approximately 1000. If the size and velocity are scaled linearly to typical microchannel values of 100μm and 1mm/s respectively (again, 10 diameters per second), the Reynolds number drops to 0.1. It quickly becomes evident that flows on the microscale are strongly dominated by viscous forces and that flow will be predominantly laminar and free of turbulence. The laminar nature of microchannel flows allows for accurate transport and deposition of biological analytes and cells for analysis (typically separation or sorting). Without turbulence however, it is difficult to obtain rapid mixing required for chemical synthesis applications [Hertzog et al. (2004), Jahn et al. (2004)]. The relatively small mixing rates associated with these

flows have led to substantial research in the area of microfluidic mixing. A review of this work is included in Chapter 2.

The aims of this thesis work are to:

1.) Develop and implement a numerical model to study the microfluidic transport phenomena of electrokinetic flows.

2.) Develop a sequential-injection based microfluidic mixing strategy and corresponding injection scheme.

3.) Identify the important operating parameters for sequential sample micromixing and establish proof-of-concept operation of the micromixing strategy through numerical modelling.

4.) Verify the numerical results experimentally using established soft-lithography techniques for microfabrication and fluorescence microscopy for analysis.

5.) Extend the micromixing design to include variable concentration modulation in the outlet stream.

6.) Develop a three-dimensional hydrodynamic focusing strategy for use with planar microfluidic geometries.

1.2 Microfluidic Transport Phenomena

Liquid flows in microchannels involve a combination of classical fluid mechanics and electrokinetics. Only a brief overview of the aspects most pertinent to this study will be will be given here, as these theories are well established. For further information the

reader is referred to quality fluid dynamics texts [Bird et al. (1960), White (1974)], and thorough electrokinetic phenomena references [Hunter (1981), Sharp et al. (2002)].

Central to electrokinetic phenomenon is the electrical double layer (EDL). When a liquid-solid phase boundary exists, electrical charges tend to be distributed in a non-uniform way near the interface due to one of four mechanisms [Hunter (1981)]:

1) differences in the affinity of the two phases for electrons,
2) differences in the affinity of the two phases for ions of one charge or the other,
3) the ionization of surface groups,
4) physical entrapment of non-mobile charge in one phase.

This non-uniform distribution of charges at the solid surface is the foundation of the electrical double layer. A schematic illustrating the non-uniform distribution of ions forming the EDL, and the resulting non-zero electrical potential distribution is shown in Figure 1.1 (figures are located at end of each chapter). The liquid ions that are in contact with the solid phase are immobilized (compact layer), whereas ions outside this range are mobile (diffuse layer). Ions in the near wall region of the diffuse layer are in a non-uniform charge distribution due to the presence of electrostatic forces, either attraction to the solid surface in the case of counter-ions, or repulsion in the case of co-ions. This non-linear distribution of ions leads to an associated distribution of electric potential which decreases as the distance from the wall increases. The magnitude of the potential at the shear plane is termed the zeta-potential (ζ_o). The diffuse layer is located between the shear layer and where the potential approaches zero in the bulk electrolyte. The size of the diffuse layer is governed by the Debye length which scales inversely with the square root of the ion concentration of the electrolyte according to [Sharp et al. (2002)]:

$$\lambda_D = \left(\frac{\varepsilon_r \varepsilon_o kT}{2e^2 z^2 Na \cdot c} \right)^{\frac{1}{2}} \qquad (1.1)$$

where λ_D is the Debye length, ε_r is the relative permittivity or dielectric constant of the liquid phase, ε_o = 8.854x10^{-12} [C/(V m)] is the permittivity of a vacuum, k = 1.381x10^{-23} [J/K] is the Boltzmann constant, e = 1.602x10^{-19} [C/proton] is the magnitude of charge on one electron or proton, z is the valence of the counter/co-ion, Na = 6.022x10^{23} [molecules/mol] is Avogadro's Number, and c is the counter/co-ion concentration.

For the applications of interest, the ion concentration is typically on the order of 100 mM or higher, resulting in a double layer thickness on the order of 10 nm. Thus the electrical double layer thickness is typically 4 orders of magnitude lower than the channel diameter.

Electroosmotic flow in a microchannel results from the motion of counter-ions in the EDL in response to an applied electric field. The fluid velocity developed along the wall in the thin EDL region is termed the electroosmotic wall velocity, $\vec{u}_{EO}$, given by the Helmholtz-Smoluchowski equation (expressed for SI units) [Sharp et al. (2002)],

$$\vec{u}_{EO} = \left(\frac{\varepsilon_r \varepsilon_\circ \zeta_\circ}{\mu} \right) \vec{E} = \nu_{EO} \vec{E} \qquad (1.2)$$

where μ is the dynamic viscosity and $\vec{E}$ is the local applied electric field strength tangential to the wall. The electric field is defined as the negative gradient of the applied potential field,

$$\vec{E} = -\Delta\Phi_{APP} \qquad (1.3)$$

where Φ_{APP} is electric potential [V]. Quite often in electroosmotic flows, there is an absence of significant pressure gradients and inertial forces due to the very small

Reynolds numbers involved. In addition, if the conductivity and zeta potential are uniform throughout, then the flow field will be mathematically similar to that of the electric field [Santiago (2001)]. No body forces act on the bulk fluid outside of the EDL because the bulk fluid is electrically neutral; however, a bulk fluid velocity is produced through viscous forces in response to the electroosmotic velocity developed in the EDL. In the case of a straight channel, the fully developed electroosmotic velocity profile is plug-like, and is shown in Figure 1.2a. The fluid in the centre of the channel is moving at the same velocity as the electroosmotic velocity at the wall. In contrast, the parabolic velocity profile developed in pressure-driven flow through a circular cross-section channel (Poiseuille flow) is given in Figure 1.2b. The plug-like velocity profile of electroosmotic flows has many advantages for microfluidic applications. The flow is strongly dependant on the electric field, which provides opportunity for direct electrical flow control via the applied potentials. In addition, the lack of cross-stream velocity gradients minimizes the dispersion of discrete samples, which is beneficial for many separation-based chemical analysis methods [Alarie et al. (2001)].

The equations governing incompressible, Newtonian, constant-viscosity fluid flow are the Navier-Stokes equation and the continuity equation [Bird et al. (1960)]. With the addition of a body force term to account for electrokinetic effects, conservation of momentum leads to the following form of the Navier-Stokes equation,

$$\rho\left[\frac{\partial \vec{u}}{\partial t} + \vec{u}\cdot\vec{\nabla}\vec{u}\right] = -\vec{\nabla}P + \mu\vec{\nabla}^2\vec{u} + \rho\vec{g} - \rho_f\vec{\nabla}\Phi_{APP} \qquad (1.4)$$

where ρ is the total mass density, P is the hydrodynamic pressure, $\vec{g}$ is the gravitational acceleration vector, and ρ_f is the net charge density (only non-zero in the EDL).

Equation 1.4 may be simplified by considering the length and timescales of the microfluidic applications of interest. The three pertinent length scales are the double layer thickness, channel hydraulic diameter, and the channel length, which are in the nanometer, micrometer, and millimeter range respectively [Erickson and Li (2002)]. Thus the channels are long, relative to their width and the flow in most cases can be expected to be axial and fully developed. The Reynolds number relates the relative magnitude of inertial and viscous effects. It is the most common dimensionless parameter associated with fluid flow and is given by:

$$\mathrm{Re} = \frac{LU}{\upsilon} \qquad (1.5)$$

where, L is the characteristic length of the flow channel [m] (used often is the hydraulic diameter, D_h), ν is the kinematic viscosity [m^2s^{-1}], and U is the average velocity [$m\ s^{-1}$]. In microfluidics, small Re values are encountered (often less than unity), indicating that the flow is laminar and dominated by diffusion (viscous effects). It is relatively common to neglect the advection and unsteady terms in these cases.

Species transport is central to the applications of interest. The equation for species transport for species, i, is given as [Bird et al. (1960)],

$$\frac{\partial c_i}{\partial t} + \vec{u} \cdot \left(\bar{\nabla} c_i\right) = D_i \bar{\nabla}^2 c_i + \frac{D_i z_i e}{kT} \bar{\nabla} \cdot \left(c_i \bar{\nabla} \Phi_{APP}\right) + R_i \qquad (1.6)$$

where, c_i is the molar concentration of species i, D_i is the ordinary diffusion coefficient, z_i is the valence of the i'th species (carries sign), T is the absolute temperature, and R_i is the volumetric rate of generation of species i by reaction. The second term from the right is the contribution from the electrophoretic migration of the charged species (the motion of charged particles in an applied electric field). In the case of fully developed flow in the

presence of an axially applied electric field, Equation 1.6 may be rearranged into the more common form,

$$\frac{\partial c_i}{\partial t} + \left(u_X + u_{PH\_i}\right)\left(\frac{\partial c_i}{\partial x}\right) = D_i \vec{\nabla}^2 c_i + R_i \qquad (1.7)$$

where u_{PH_i} is the electrophoretic velocity of the i^{th} species in the axial direction, given by,

$$u_{PH\_i} = \nu_{PH\_i} E_X = \left[\frac{D_i z_i e}{kT}\right] E_X \qquad (1.8)$$

where ν_{PH_i} is termed the electrophoretic mobility.

For the cases studied in this thesis, contributions from electrophoretic mobility have been neglected with the assumption that the species is neutral (z_i=0) and no reactions take place (R_i=0). The appropriate form of the species transport equation is,

$$\frac{\partial c_i}{\partial t} + \vec{u} \cdot \left(\vec{\nabla} c_i\right) = D_i \vec{\nabla}^2 c_i \qquad (1.9)$$

The mass-based Peclet number is used in this thesis to relate the ratio of mass transport by advection to that by diffusion. The Peclet number is the product of the Reynolds number and Schmidt number, and is given as:

$$\mathrm{Pe} = \mathrm{Re} \times \mathrm{Sc} = \frac{LU}{\upsilon} \times \frac{\upsilon}{D} = \frac{LU}{D} \qquad (1.10)$$

A high value for the Peclet number describes a system where the advective transport of mass dominates. Peclet numbers in this thesis range in value from 1 to 10 000.

Due to the small scales associated with microsystems, it is important to verify that the fluid can be modeled as a continuum. The Knudsen number represents the ratio

between the average distance traveled between molecular collisions in a fluid and the size of the system. It is defined as [Nguyen and Wereley (2002)]:

$$Kn = \frac{\lambda}{L} \tag{1.11}$$

where λ is the mean free path, and L is the characteristic length scale of the system. For Knudsen number values greater than approximately 10, individual molecular interactions are significant. However, for liquid water the mean free path is only 2.5Å, which would require a length scale of much less than 1 nm for individual molecular interactions to be significant. In this thesis, the smallest length scale studied is 16μm, so the continuum assumption when modeling is quite valid in these cases.

1.3 Microfluidic Methodologies

Research in the field of microfluidics is predominantly performed in one of three main areas: numerical simulations, microfabrication techniques, and experimental investigations. Due to the inherent length scales, the manufacturing of microchannels and subsequent running of experiments can be difficult and expensive. In the absence of turbulent effects, numerical simulations can provide highly accurate and well resolved data in a timely manner with large computational resources. Thus, quite often in microfluidics, as with this work, the first stage of research involves a numerical study. Recently, efficient and inexpensive methods have been developed for the manufacturing of microchannels and microchannel networks [McDonald et al. (2000)]. The advancements made in microfabrication have allowed for a dramatic increase in the number and complexity of experiments that are being performed. A clean room is no

longer required in order to fabricate custom microfluidic networks. A variety of experimental techniques for microfluidics research are available, most are based on direct visualization through fluorescence microscopy [Sinton (2004)]. In this thesis, all three of these methodologies have been utilized in the development of a sequential sample micromixer and three-dimensional focusing device.

1.3.1 Numerical Method

Computational fluid dynamics modelling has proven to be an excellent tool for providing insight into transport phenomena in microsystems [Erickson et al. (2003a), Bianchi et al. (2000), Ermakov et al. (2000, 1998), Patankar and Hu (1998)]. Although most microflows are free of turbulence, modelling challenges arise due to the increased role of surface/electrokinetic phenomena and the mixture of pertinent length scales in these flows [Erickson and Li (2002)].

1.3.1.1 Equations and Assumptions

In the numerical model employed in this work, the electrical double layer which facilitates electroosmotic flow is not resolved. A typical Debye layer thickness for aqueous solutions is on the order of nanometers and the microchannels studied here have features on the order of tens of micrometers. For low Reynolds number electroosmotic flows, in which viscous and Lorentz forces dominate, the fluid velocity at the wall can be prescribed as a boundary condition using the Helmholtz - Smoluchowski equation (Equation 1.2).

The electric field is not influenced by the concentration field as the electrical conductivity is assumed to be uniform throughout. As a result, it is only necessary to solve the electric field for each unique set of applied electrical potentials, and it can be decoupled from both the fluid flow and species transport equations [Ermakov et al. (1998), Patankar and Hu (1998)]. By extension, the flow field depends only on the applied field and can be solved independently from the concentration field. By solving each equation in sequence, solutions may be obtained more efficiently.

The electric field is the first equation to be solved and is obtained from the distribution of the applied electric potential, Φ_{APP}, according to,

$$\vec{E} = -\nabla\Phi_{APP} \tag{1.12}$$

where the electric potential is determined from the Laplace equation.

$$\nabla^2\Phi_{APP} = 0 \tag{1.13}$$

The interior flow field is then solved using the continuity and Navier-Stokes equations,

$$\nabla \cdot \vec{u} = 0 \tag{1.14}$$

$$\rho\left(\frac{\partial\vec{u}}{\partial t} + (\vec{u}\cdot\nabla)\vec{u}\right) = -\nabla p + \mu\nabla^2\vec{u} \tag{1.15}$$

where, ρ is the density and p is the pressure. The Lorentz force term in Equation 1.4 is implemented here as a boundary condition for velocity. Specifically, the local fluid velocity is prescribed using the Hemholtz - Smoluchowski equation (Equation 1.2) and the local applied electric field strength. Solving the Navier-Stokes equations for the flow field was the most straightforward way to implement this model in the commercial code.

However, due to the low Reynolds number, the inertial terms contribute relatively little and the velocity field. The model also contains a species transport equation which governs the advection and diffusion transport of individual species.

$$\frac{\partial c}{\partial t} + (\vec{u} \cdot \nabla)c = D\nabla^2 c \qquad (1.16)$$

Here, c is the concentration of the species.

For some of the processes to be studied in this work, rapid switching of the electric fields is required. When the applied potentials are switched, changes in the velocity field are considered to occur instantaneously, requiring that fluid inertia be neglected. This assumption is valid due to the relatively small timescale required for momentum diffusion in the cross-stream direction [Santiago (2001)]. The development time can be estimated as:

$$\tau = \frac{\rho D_h^2}{\mu} \qquad (1.17)$$

which, for the dimensions employed, is on the order of milliseconds. This development time is small compared to the timescale associated with the switching of the applied electric field (0.1 to 1 seconds).

1.3.1.2 Finite Element Mesh Analysis

The finite element meshes used for the numerical aspects of this work were chosen based on successive refinements toward a grid independent solution. In the processes studied, concentration is the most grid-demanding variable due to the large gradients encountered throughout the domain. In addition, concentration is the most

critical output, as its solution is dependant upon the solutions of both the velocity and the electric field. A mesh study was performed to examine the optimum element size to be used in high concentration gradient regions, while maintaining reasonably fast convergence times. A 2-D model of a 100μm by 1mm channel was used with an electroosmotic flow entering at 1mm/s. The inlet concentration was instantaneously changed from c = 0 to c = 1 at time t = 0s. The maximum concentration found in the system a short time later (t = 0.2s) was used as a measure of the numerical error produced. The maximum concentration can deviate from the physical maximum (c = 1) due to interpolation errors between sharp gradients. This numerical artifact is common in time dependent solvers and is a clear indication of an insufficient discretization. The results for the different meshes studied are shown in Table 1.1 with a corresponding plot shown in Figure 1.3. It was determined from this study that accurate results (errors less than 1%) can be obtained for the processes studied when elements less than 10μm in size are used in high concentration gradient regions. The role of time step is demonstrated in mesh analysis cases 5 and 6, using a ten times longer maximum time step (0.01s). Compared to otherwise similar cases 3 and 4, cases 5 and 6 exhibit errors that are 2 orders of magnitude higher. Also, taking into account the amount of time required to obtain a converged solution, mesh analysis case 4 is the most appropriate choice for these studies.

Mesh Case	Element Size (μm)	Max Time Step (s)	Solution Time (s)	Error (%)
1	38	0.001	20	10
2	19	0.001	35	3
3	9	0.001	87	0.4
4	4.5	0.001	370	0.1
5	9	0.01	53.8	45
6	4.5	0.01	273	25

Table 1.1 A summary of the important parameters used for each mesh case during the mesh analysis.

Additional numerical challenges arise with the production of singularities when solving for the electric field around interior bends greater than 180 degrees. This is a well documented problem in numerical simulations and is discussed with respect to microfluidic systems by Patankar and Hu (1998). The effect of the singularities was minimized by locally refining the grid and rounding the corners (in practice such are naturally rounded due to the manufacturing process). Ensuring overall mass conservation provided additional validation. Ultimately, however, the numerical results were used to guide the design of the prototype chip and establish suggested operation parameters and performance expectations. The operation performance of the resulting prototype chip was generally in keeping with the numerical results, and the numerical results were validated in that context.

1.3.2 Microfabrication

The production of microchannels and microchannel networks requires manufacturing methods capable of producing feature sizes on the order of micrometers.

Conventional methods are not suitable for production on this scale. Current microfabrication techniques include micromachining, laser etching, chemical etching, and imprint lithography. Many of these techniques are time consuming and require a clean room to be performed properly. The single most significant innovation in microfluidics over the past decade has been the methods for fabrication of microfluidic devices from soft polymeric materials [Kamholz (2004)]. In recent years, the development of soft-lithography based microfabrication techniques have become extremely popular. For these methods, a clean room no longer required and the turnaround time for the complete concept-to-prototype chip is less than 24 hours [McDonald et al. (2000), Duffy et al. (1998)].

Soft-lithography can be divided into the four main steps presented in Figure 1.4. The first step is to make the photomask. The desired microchannel pattern is produced using a CAD program, and then using a high resolution printer, it is transferred onto a transparency. The transparency acts as a photomask. A uniform layer of photoresist is spun onto a microscope slide. The thickness of this layer is the ultimate thickness of the microfluidic channel structure. High intensity, columnated UV light passes through the photomask, and selectively exposes the photoresist. The UV light cures the photoresist, so that upon development, all unexposed photoresist is dissolved, leaving only a positive-relief structure of the original pattern (referred to as the master). In the third step, the microchannels are produced by curing a liquid polymer, poly-dimethylsiloxane (PDMS), against the master and producing a negative imprint of the pattern. The final step is to punch reservoir holes and seal the PDMS imprint to a clean glass slide.

1.3.3 Experimental Method

The experiments performed in this work use established fluorescence microscopy techniques, modified slightly for microfluidics use, which can be divided into 4 main aspects: working solutions, electrical aspects, fluorescence microscopy and image processing. The experimental setup is shown in Figure 1.5. In a typical experiment, the microchannel is filled with an aqueous solution containing dilute concentrations of a fluorescent dye. The solution flows electrokinetically and is visualized using fluorescence microscopy. The solutions are continuously excited by light from the microscope (green) and the resulting fluorescent emission (red) is imaged through the microscope onto an 8-bit black and white CCD camera. The resulting image is numerically processed such that the intensity of each pixel is converted to a value representing the normalized concentration of the fluorescent solution at that location.

1.3.3.1 Working Solutions

The working fluid in all cases was an aqueous buffer solution, typical of the majority of microfluidic applications. The buffer solution acts to stabilize the pH of the solution at a prescribed value. This stabilization mechanism is important as both the intensity of the fluorescence emission and electrokinetic phenomena are sensitive to pH. One side effect of electrokinetic flow is that water is electrolyzed at the electrode reservoirs, producing an acidic solution at the anode (due to the production of protons), and, conversely, a basic solution at the cathode (due to the production of hydroxyl ions). The buffer works to stabilize the pH in both cases.

The physical and thermal properties of the solution are well approximated by those of pure water (density, viscosity, thermal conductivity, heat capacity) due to the dilute nature of the solutions (100mM max concentration). The electrical conductivity, which is a strong function of ionic concentration, is an exception. Fluorescent dye was only added in dilute amounts with respect to the buffer, to ensure that its addition did not significantly effect the ionic concentration of the solution. Care was taken during the preparation of different solutions that ionic concentrations were equal. Immediately before use, all solutions were filtered using 0.2-μm pore size syringe filters. Specific details on the concentrations and ionic strengths will be provided separately later in the context of each experimental run.

1.3.3.2 Electrical Aspects

The high electric field strengths required to produce electroosmotic flow (approximately 100V/cm for 1mm/s) were generated using a high-voltage power supply (Spellman - SL30). For the operation of the microfluidic chips, independent control of up to four potentials was required. In addition, to accomplish multi-step processes, time-dependent control for two separate voltages and rapid switching between modes must was required. It was desired to facilitate a rapid two-step process, with switch timing externally controlled from a PC. The voltage circuitry is essentially multiple paths of resistors in series with a potentiometer as the top resistor in each current path. The potentiometers, provided individual electrode voltage adjustment, and were used to 'tune' the flow. A schematic of the switching circuitry is shown in Figure 1.6. The circuit uses a two step approach for switching the reservoir potentials due to the large difference

between the input and output potentials (5V TTL in, ~1kV out). A 5 Volt TTL signal from Labview is used to accurately trigger a silicon transistor (TIP110) which in turn applies a 12VDC supply to the mechanical relay. The mechanical relay is capable of switching 2 sets of 4 reservoir potentials at rates of ~25 Hz. A diode is placed across the coil of the mechanical relay in order to protect the transistor, shown in the schematic in Figure 1.6. Under normal operation the diode will not conduct, current will only flow through the diode immediately after the transistor is switched off. At that moment, current tries to continue flowing through the relay coil and it is harmlessly diverted through the diode. Without the diode no current could flow and the coil would subject the transistor to a damaging high voltage spike.

1.3.3.3 Fluorescence Microscopy

Fluorescence microscopy is commonly used in biology as a means of visualizing the components of cells. The process is well established and is easily adapted for use with microfluidic studies. Fluorescence is an optical phenomenon that occurs when a molecule absorbs a high-energy photon and re-emits it as a lower-energy (longer-wavelength) photon. The energy difference between the maximum absorbance wavelength and the maximum emission wavelength is termed the Stokes shift, and is particular to the fluorophore being excited. For the studies performed here, Rhodamine-B is used as the fluorescent molecule. Under typical conditions, the absorption maximum of the Rhodamine-B molecule is 550 nm (green), and the emission maximum is 605 nm (orange/red). This shift in maxima allows for selective filtering of the absorption and

emission light so that only the fluorescent emission signal reaches the camera. A schematic of the filtering process is shown in Figure 1.7, with filters specific to the wavelengths encountered with Rhodamine-B. It is important to note that the fluorescent lifetime (1-10 ns) is insignificant with respect to timescales of microflows.

1.3.3.4 Image Processing

Images of the microchannel taken with the CCD camera can include variations in intensity levels due to a non-uniform distribution of the excitation light, the presence of ambient lighting, and curved surfaces within the channel. These variations are artifacts of the imaging process and do not represent concentration variations within the solution. In order to be able to relate the pixel intensity to the fluorophore concentration it is essential to digitally post-process the images to remove these artifacts. The image processing method is illustrated in Figure 1.8. The first step in processing the images is to normalize each pixel with respect to the full range of intensities encountered during operation. The lowest intensity level is found for each pixel using a dark field image (which is taken when no fluorescent dye is passing through the system) and the highest possible intensity is found using a bright field image (which is taken when the system is flooded with the fluorescent solution). All fluorescent intensity data will fall between these two levels during operation, as shown in Figure 1.8a. For each pixel, the raw data is normalized using the equation [Inoue and Spring (1997)]:

$$\text{Normalized Data} = \frac{\text{Bright Field - Raw Data}}{\text{Bright Field - Dark Field}} \qquad (1.18)$$

Once normalized, the data will have a value between 0 and 1, and is equivalent to a dimensionless form of the fluorescent dye concentration. In addition to normalizing the data, a smoothing function is also performed. Minor variations in the CCD sensitivity can produce intensity spikes in the normalized data shown as the dotted line in Figure 1.8b. The smoothing function averages each pixel's intensity with the intensity of its neighbours using a weighting function based on distance. The result is that sharp changes in intensity are damped and the data is more representative of the physical case. The relative change in the pixel intensity values before and after smoothing provides a measure of the imaging-induced error. In the cases studied here, the maximum imaging-induced error was approximately ±2.5% (of full scale), with typical values within the range of ±1% (of full scale).

1.4 Overview of This Thesis

The high degree of interest in this field has produced and exponential increase in the number of contributions to the literature over the past 10 years [Kamholz (2004)]. This is further evidenced by the number of contributions referenced in this thesis that were published post 2003, the year this thesis was begun. The work in this thesis has resulted with prompt contributions to the literature [Coleman and Sinton (2005a – available online), Coleman et al. (2005b - submitted)] and in conference proceedings [Coleman and Sinton (2004), Coleman et al. (2005c,d)]. The specific contributions of this thesis are summarized below:

In Chapter 1, the aims and motivation of the thesis work were presented. Next a brief overview of microfluidic transport phenomena was presented as well as a description of the numerical, microfabrication and experimental methodologies used when performing this research. Although the novel electrokinetic processes developed through this thesis (Chapters 2 and 3) are the primary contributions, building up the core capabilities of the microfluidics lab, particularly the numerical and experimental methods, is a lasting, albeit local, contribution of this thesis work.

In Chapter 2, a numerical model is developed for the study of discrete sample mixing and the governing parameters involved. The model is extended to develop and evaluate a sequential sample injection strategy that is coupled with an expansion region. An experimental investigation is performed based on the design developed through the numerical results. Proof-of-concept operation is established and a set of preferred operating parameters are described. The experiments are extended to demonstrate accurate control and readily variable outlet concentration.

In Chapter 3, a numerical model is developed for the study of a three-dimensional hydrodynamic focuser for microfluidic applications. Electrokinetic flow is used with strategic surface charge patterning to induce localized flow circulations in a planar geometry.

In Chapter 4, a brief overview of the key contributions of the thesis is given, and a summary of future projects stemming from these findings are proposed.

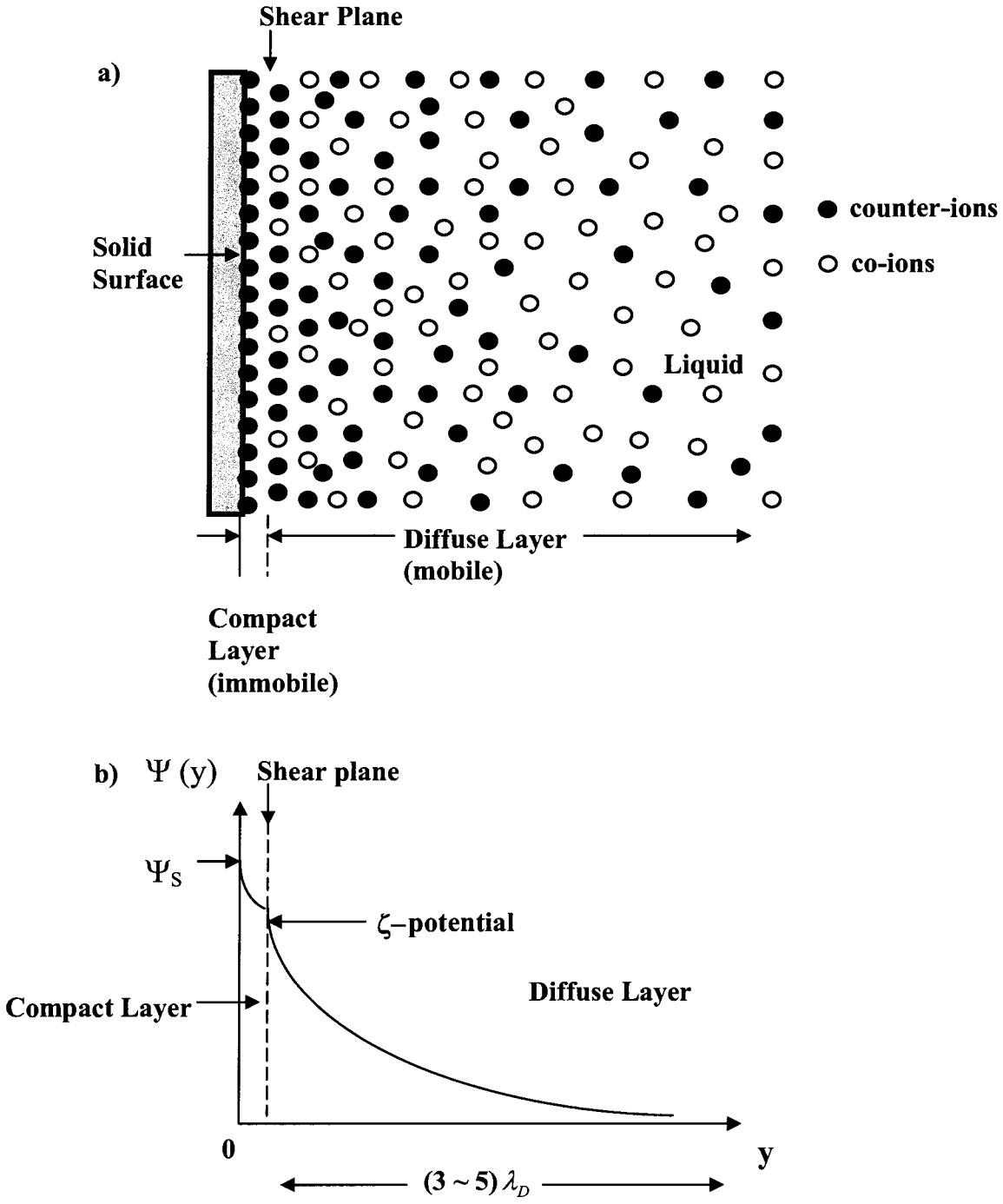

Figure 1.1 Schematic of: (a) the non-uniform ion distribution near the solid surface which forms the electrical double layer (EDL); and (b) the potential distribution in the EDL.

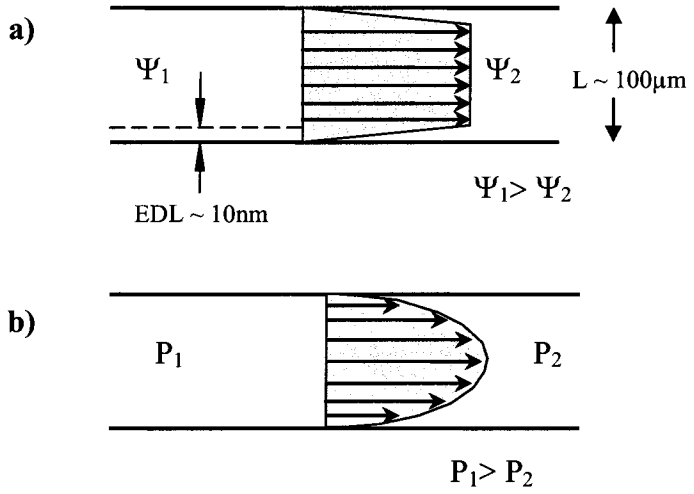

Figure 1.2 Cross-stream velocity profiles in a circular cross-section microchannel characteristic of: (a) electroosmotic flow; and (b) pressure-driven flow.

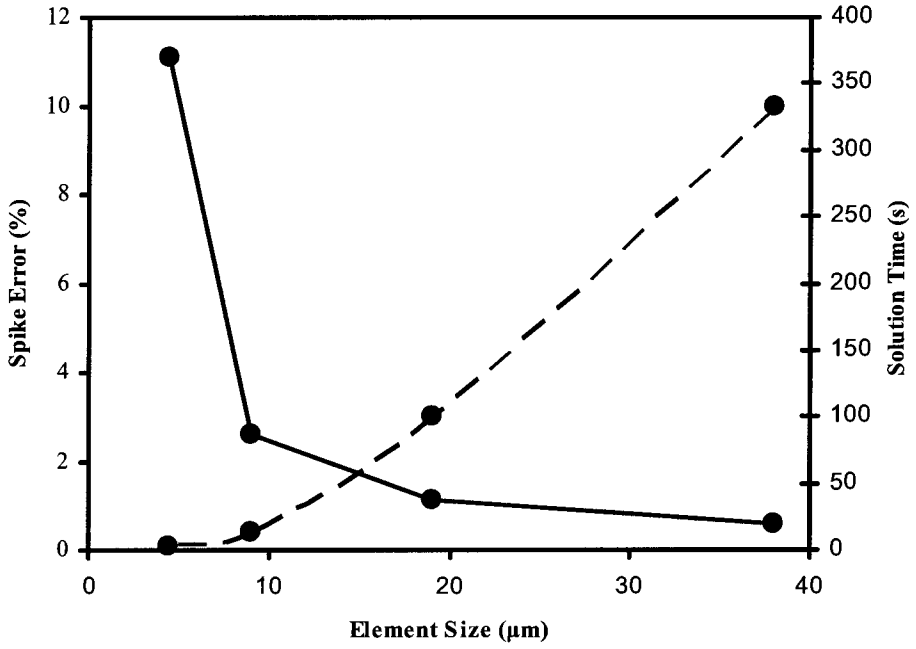

Figure 1.3 The percentage error (dash) and convergence time (solid) are plotted with respect to the maximum element size for mesh analysis cases 1 - 4.

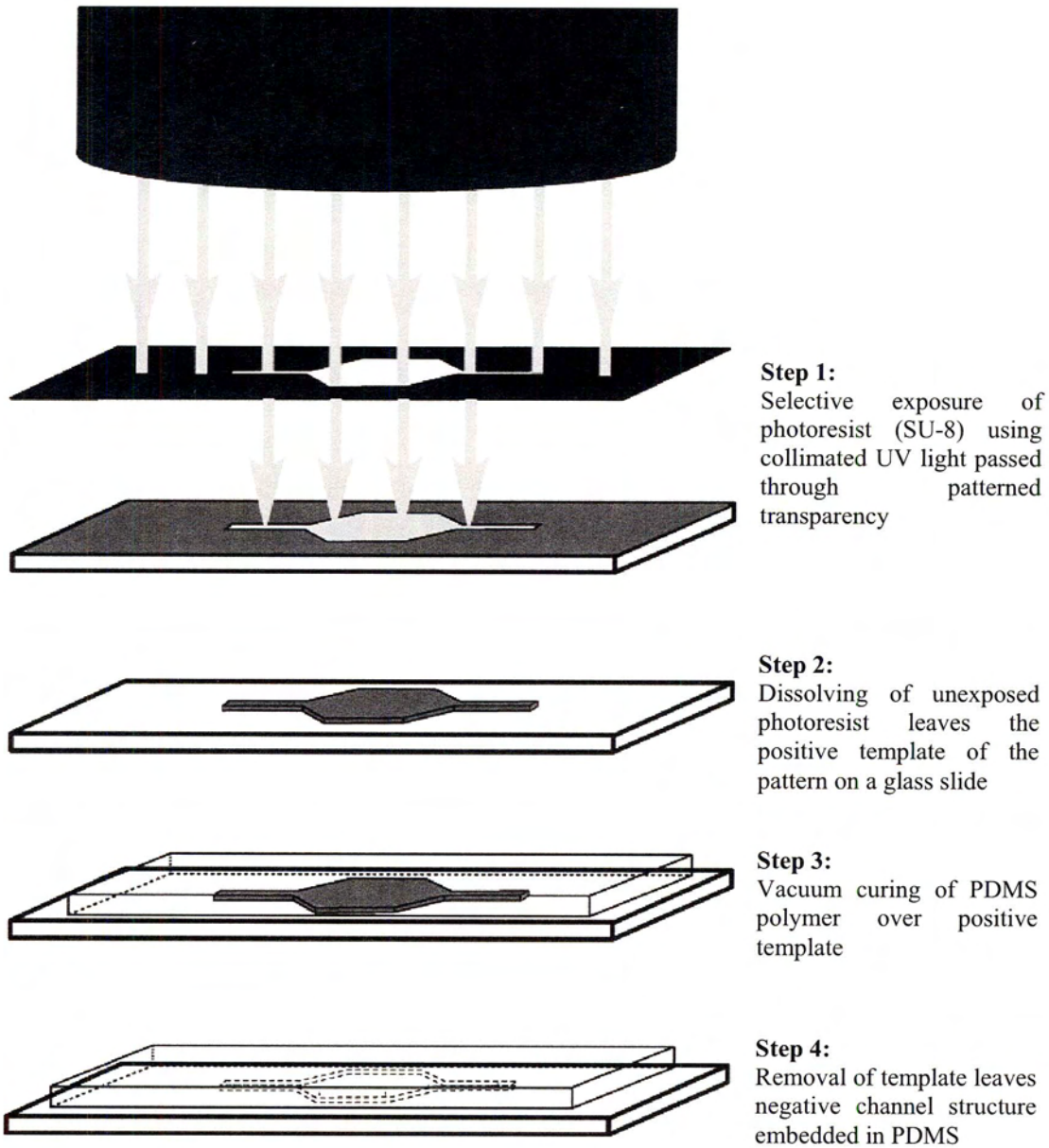

Figure 1.4 Schematic and description of the soft-lithography microfabrication method.

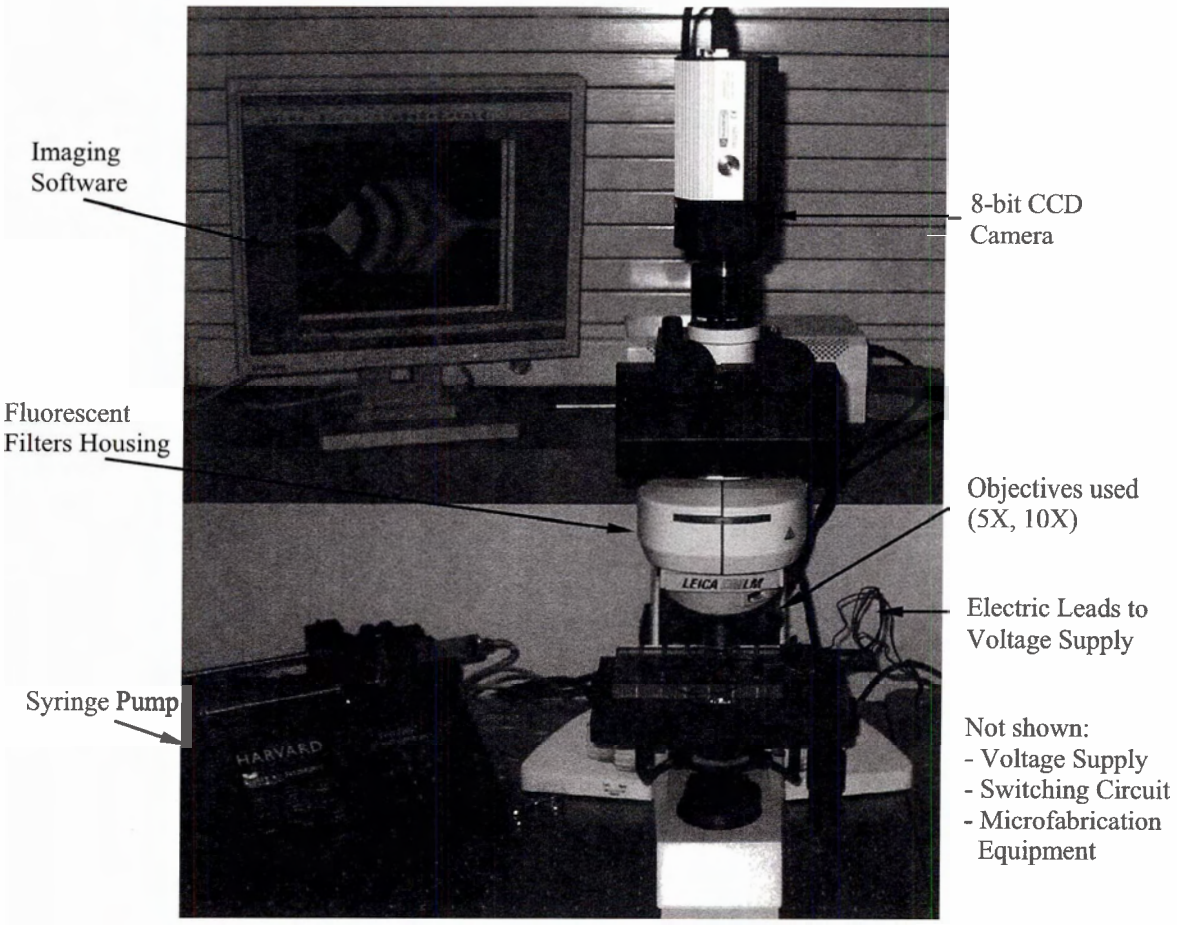

Figure 1.5 Labeled photograph of the experimental setup used in this thesis.

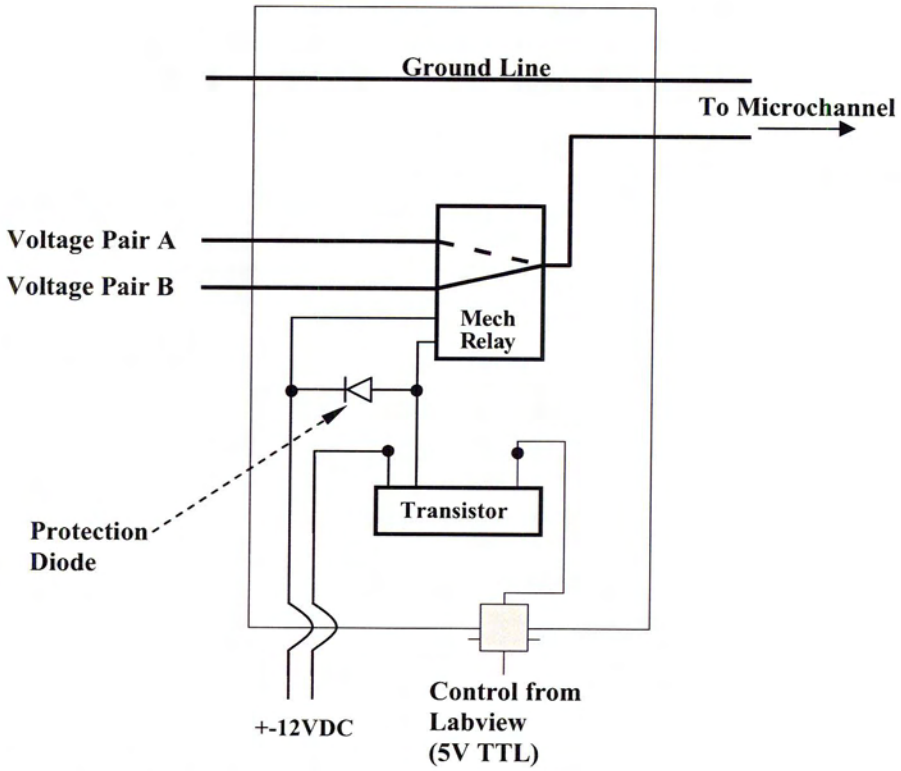

Figure 1.6 Switching circuit diagram.

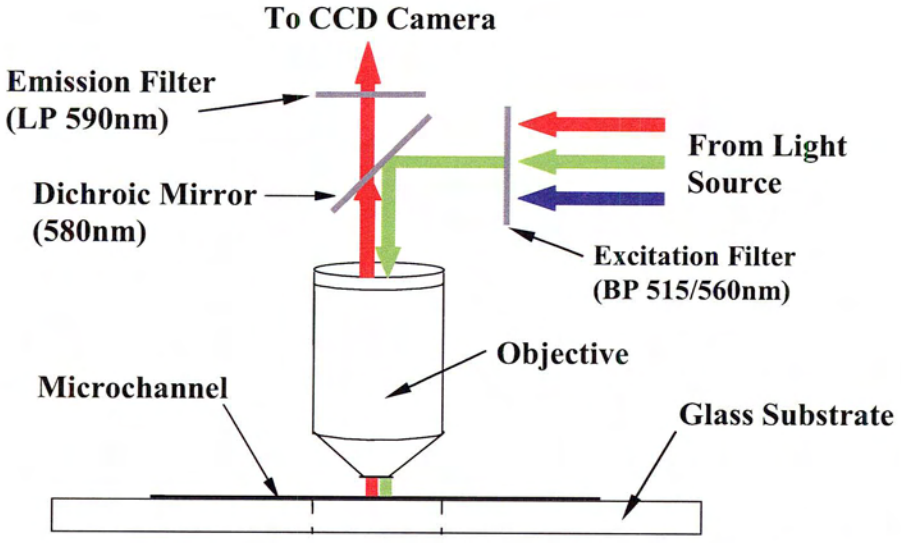

Figure 1.7 Schematic of the fluorescence microscopy setup. The filters shown demonstrate the light interactions encountered with Rhodamine-B fluorescent solution.

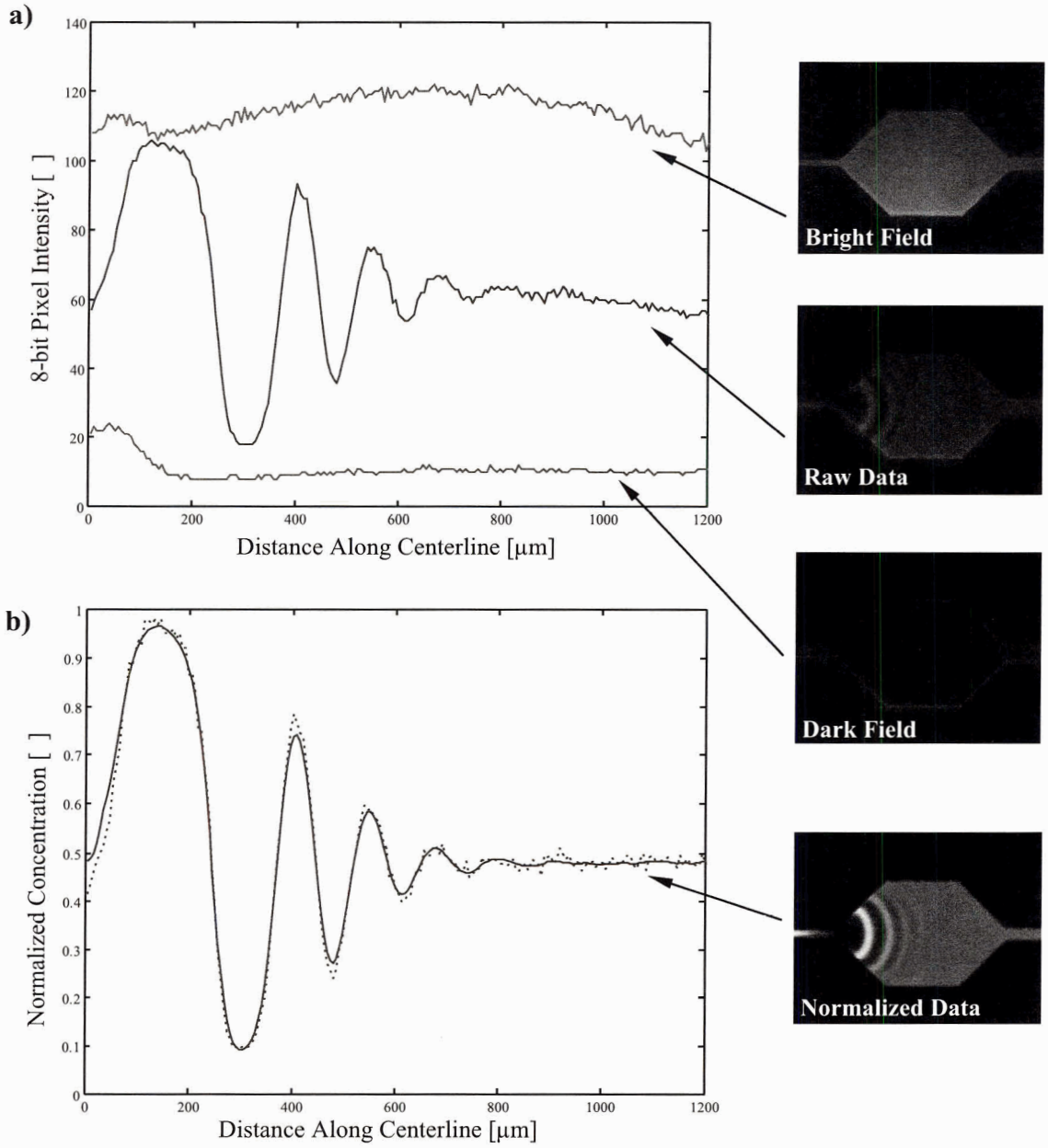

Figure 1.8 In a), pixel intensity profiles are plotted along the centerline of the raw data, bright field and dark field images. In b), concentration profiles are shown along the centerline for the processed data after normalizing (dot) and after both normalizing and smoothing (solid). Shown at right are the corresponding images.

Chapter 2

ELECTROKINETIC MICROFLUIDIC MIXING

In this chapter, a new microfluidic mixing strategy is developed which exploits stream-wise diffusive mixing of a sequence of injected samples in an electroosmotic flow. Numerical simulations demonstrate the method and predict its performance. Sequential injection micromixing is first considered using ideal concentration inputs to study the effects of geometry and switch frequency. To facilitate sequential injection on-chip, new sequential injection schemes are developed and coupled with an expansion region. Next, an experimental study is performed on the symmetry-based sequential injection microfluidic mixer. The microfluidic chips for this study are manufactured in polydimethylsiloxane (PDMS) using established soft-lithography based microfabrication methods. Fluorescence microscopy is employed to analyze, quantify and demonstrate the effectiveness of this mixing strategy, as well as to determine an optimal frequency range for operation. In addition, it is demonstrated experimentally that that outlet concentration can be actively controlled by adjusting the duty cycle of the applied switch frequency.

2.1 Background: Microfluidic Mixing

Flexible and effective microfluidic mixing, typically of reagents and sample, is central to many on-chip analytical processes [Nguyen and Wu (2005), Stone et al. (2004)]. To date, research in the area of fluid mixing in microchannels has focused on two, rather different, objectives. One goal has been to minimize the axial broadening and dissipation of discrete samples during transport and/or separation in the streamwise direction, while a second common objective has been to maximize cross-stream mixing of two adjacent laminar streams. Microfluidic mixing is typically limited to diffusion due to the laminar nature of microflows. Strategies to increase stream-stream mixing have focused on increasing both concentration gradients and the interfacial area available for diffusion [Stone et al. (2004)]. Mixing strategies are commonly divided into two categories: active and passive. Active mixers utilize external forces such as modulating pressures [Deshmukh et al. (2000), Glasgow and Aubry (2003), Glasgow et al. (2004a)] or oscillating electric fields [Oddy et al. (2001), Tang et al. (2002), Glasgow et al. (2004b), Lin et al. (2004a)] whereas passive mixers [Jacobson et al. (1999), Liu et al. (2000), Johnson et al. (2002), Stroock et al. (2002), Erickson and Li (2002), Biddiss et al (2004), Hertzog et al. (2004)] utilize cross-stream diffusion and, in some cases, strategic surface patches or geometries to introduce chaotic advection within the flow.

The most basic passive mixer is the T-mixer, in which two adjacent laminar streams mix via cross-stream diffusion [Jacobson et al. (1999)], and relatively long mixing channels are required to attain high mixing efficiencies. A number of strategies have been developed to increase the mixing rate in T-mixers. Recent studies have found that the mixing rate can be increased by promoting cross-stream transport of the fluid

with strategic patterns of non-uniform surface charge along the channel walls [Biddiss et al (2004), Erickson and Li (2002)]. Similar results for pressure-driven flows have been obtained using asymmetric grooves cut into the base of the microchannel [Johnson et al. (2002), Stroock et al. (2002)].

Applying alternating driving forces at each fluid inlet is an active mixing technique that is attractive due to its relative simplicity. Deshmukh et al. (2000) first utilized pulsatile micropumps to achieve increased interfacial area for mixing between two laminated microfluidic streams. Glasgow and Aubry (2003) also applied pulsatile pressure-driven flow to improve mixing of a microfluidic stream with a perpendicularly connected inlet. Glasgow et al. (2004a) elaborated on their technique, achieving mixing efficiencies up to 84%. In the context of electrokinetic flows, the driving electrical potentials may be varied to enhance mixing. These mixers require no moving parts, and no additional components other than external circuitry. Tang et al. (2002) first achieved spatial composition modulation in the outlet of a T-form mixer by alternating the application of the potentials between inlet reservoirs. Glasgow et al. (2004b) demonstrated significantly enhanced microfluidic mixing using alternating voltages at the inlets of a T-form mixer. With 90° out of phase pulsing they predicted numerically that this technique could achieve over 80% mixing, in qualitative agreement with their experimental results. Lin et al. (2004a) also presented a microfluidic T-form mixer utilizing alternately switching electroosmotic flow. Applying the driving potential to each inlet in turn, while allowing the other inlet electrode to float, was shown to produce a modest increase in mixing efficiency over the static case. Applying a 'pinched voltage'

(analogous to 'pull-back' voltages described in microfluidic dispensing works [Ermakov et al. (2000)]) they reported 97% mixing with optimized operating parameters.

The threshold requirement for mixing efficiency varies from application to application. For instance, a 90% concentration change in local denaturant is sufficient to initiate folding for most proteins [Hertzog et al. (2004)], and it is the timescale associated with that local concentration change that is more critical for that particular micromixing application. In the context of on-chip solution preparation for micro-total-analysis systems, however, high mixing efficiencies, steady outlet flow, and short axial length are generally desirable [Nguyen and Wu (2005), Stone et al. (2004)]. The inherent asymmetry of mixing strategies based on T- and Y-form geometries leads to small cross-stream concentration gradients that are difficult to reduce. For example, to increase mixing efficiency from 90% to 99% in a basic electrokinetic T-mixer requires a 40% increase in axial length.

In general, the time required for the diffusive mixing of two co-laminar streams scales quadratically with the width of the channel according to [Johnson et al. (2002)],

$$t_{cross} \sim \frac{w^2}{D} \tag{2.1}$$

where t_{cross} is the time required to obtain cross-stream mixing, w is the width of the channel and D is the diffusion coefficient. In contrast, in discrete sample transport the concentration gradients are located primarily in the streamwise, or axial, direction. The time required to disperse/mix a discrete sample scales quadratically with the length, l, of the sample. As a discrete sample enters an expansion chamber, the length varies inversely

with channel width and the time required for steam-wise mixing (t_{stream}) may be expressed as:

$$t_{stream} \sim \frac{l^2}{D} \sim \frac{1}{Dw^2} \qquad (2.2)$$

In effect, increasing the sample width decreases the distance through which diffusion must occur and increases the axial concentration gradients.

2.2 Numerical Model

An overview of the numerical model used in this study is outlined in section 1.3.1. Only the details specific to this study are included here. The model was implemented in two dimensions using *FEMLAB 3.1*. For low Reynolds number electroosmotic flows with uniform surface charge and no pressure gradients, the velocity field is mathematically similar to the electric field [Santiago (2001)] allowing for an accurate two-dimensional representation. The electric field and flow field equations are solved at steady-state using the direct (UMFPACK) solver. For species transport, a time dependent solver was used with an imposed maximum allowable time step of 0.001s. Care was taken during mesh generation to ensure that proper mesh refinements were made in regions where velocity and concentration gradients are large (see section 1.3.1.2 for mesh analysis). For the electric field boundary conditions, potentials were assigned at the channel inlets, electrical ground was assigned at the outlet and zero flux was assigned at the walls. The boundary conditions for the flow field were zero pressure at the inlet and outlet with a wall velocity boundary condition applied using the Helmholtz-Smoluchowski approximation (Equation 1.2). Finally for species transport, zero flux was

imposed at the walls, a constant concentration was imposed at the inlets and a convective-only flux boundary condition was applied at the outlet. The physical properties of the solutions were taken to be those of water, and a diffusion coefficient of $D = 2x10^{-10}$ m^2s^{-1} and an electroosmotic mobility of $3.48x10^{-8}$ $m^2V^{-1}s^{-1}$ (corresponding to a zeta potential value of ζ_o = -50mV) were assigned.

In order to quantify the degree of mixedness, the concentration profiles at the exit were normalized using an equation similar to that used by Jeon et al. (2000). This equation quantifies the amount of mixing based on the standard deviation of the concentration profile from that of the perfectly mixed case. A perfectly mixed solution at the outlet would therefore have a *%Mixed* value of 100%, where *%Mixed* is defined as,

$$\%Mixed = \left(1 - \frac{\sqrt{\frac{1}{N}\sum_{i=1}^{N}(c_i - \bar{c})^2}}{\sqrt{\frac{1}{N}\sum_{i=1}^{N}(c_i^o - \bar{c})^2}}\right) \times 100 \qquad (2.3)$$

where N, c_i, c_i^o, and $\bar{c}$ are the total number of points examined in the cross-stream direction, the concentration at each point, the concentration at each point if no mixing were to have taken place, and the concentration of the perfectly mixed case, respectively. The variable $\bar{c}$ can also be described as the mean concentration of the bulk fluid. At any location, values for c_i^o (the concentration at each point if no mixing were to have taken place) switch between c* = 0 and c* = 1 as injections flow past. In practice it is not necessary to explicitly calculate c_i^o because both injections of c* = 0 and c* = 1 result in a constant denominator value of 0.5 in Equation 2.3.

2.3 Numerical Results and Discussion

2.3.1 Axial Mixing of Ideal Sequential Injections

Microfluidic mixing through sequential injection was first studied with a simple expansion chamber, assuming an ideal binary injection scheme at the inlet. The value for concentration at the inlet boundary followed a time dependant square wave which oscillated between the normalized concentrations of $c^* = 0$ and $c^* = 1$, where $c^* = c/c_o$, $c = c_o$ for the original concentration of solution A, and $c = 0$ for solution B. In an effort to reduce numerical errors, a Heaviside function was applied to smooth the corners of the square wave and provide a continuous first derivative of the function. The inlet flow was constant at a velocity of 1mm/s, carrying equal volumes of solution A and solution B, in sequence. The switch frequency was adjusted to control the length of the injected samples. For example, for simulations with a switch frequency of 1Hz, the resulting samples had a length of 1mm. The concentration fields produced with three different configurations are shown in Figure 2.1. Axial concentration profiles are plotted for the channel centerline and the 2-D concentration fields are shown inset. In Figure 2.1a, results are shown for a 2mm expansion chamber with samples 1mm in length. The peak concentration was reduced along the centerline from $c^* = 1$ at the inlet to $c^* = 0.71$ at the outlet. The effect of increasing the length of the expansion region is shown in Figure 2.1b where, with a 5.5mm expansion, the peak concentration was further reduced to a maximum of $c^* = 0.58$. The effect of increasing the injection frequency (and subsequently decreasing the injected sample length) is dramatic. This effect is shown in Figure 2.1c, where mixing is effectively complete only 200μm into the expansion region.

The low magnitude concentration spikes in Figures 1a and b, where $c^* > 1$ and $c^* < 0$, are numerical errors produced by the nearly instantaneous concentration changes occurring between injections. These spikes diffuse quickly and have a negligible effect on the final mixed solution.

If the outlet stream is not mixed to equilibrium, then the concentration profiles at the outlet will vary both temporally and spatially. In Figure 2.2, cross-stream concentration profiles at the outlet of the mixer (shown in Figure 2.1a) are plotted at 10 equal intervals over the two second injection period. At the outer edges of the channel, the solution is well mixed with concentrations oscillating between $c^* = 0.47$ and $c^* = 0.53$. Temporal fluctuations are greatest along the centreline of the outlet where the concentration oscillates between $c^*=0.36$ and $c^*=0.64$. The discrepancy between the mixedness of the near-wall fluid and that of the centreline is due to the velocity field. The fluid traveling along the outer regions of the expansion takes longer to reach the outlet. This increased residence time in the expansion chamber results in increased axial mixing and reduced concentration fluctuations near the wall in the re-focused flow. Although cross-stream concentration gradients in the outlet will induce further mixing, the preferred strategy is to eliminate all temporal and spatial concentration differences as in the case shown in Figure 2.1c.

2.3.2 On-Chip Sequential Injection Micromixing

Several on-chip injection schemes have been developed, including the pinched injection [Alarie et al. (2001), Jacobson et al. (1998)], the gated injection scheme [Ermakov et al. (2000)], and more recently, dynamic three-step injection techniques

[Sinton et al. (2003a), Sinton et al. (2003b)]. Each of these is based on single sample injection, primarily driven by on-chip capillary electrophoresis applications. In addition to these, sequential injection schemes have been developed for pressure driven flows [Deshmukh et al. (2001), Fujii et al. (2003)] as well as for electroosmotic flows [Tang (2002)]. Based on T- or Y-channel configurations, these sequential injectors produce injections which are non-uniform in the cross-stream direction. When combined with an expansion channel for the purposes of mixing, these non-uniformities result in lingering cross-stream gradients and reduced mixing efficiency. Two new sequential injector designs are presented here which minimize the magnitude of the cross-stream concentration gradients produced. Both designs maintain a constant outflow of mixed solution which is well suited for applications where the continuous flow of a mixed solution is required. The first sequential injector studied uses a microchannel cross to produce sequential streams in two outlet channels simultaneously. The second injector also uses a microchannel cross, but with three inlet channels in a symmetric fashion, and a single outlet channel.

2.3.3 Dual Outlet Sequential Injector

The operation of the dual outlet sequential injection micromixer is presented in Figure 2.3. The two electric fields applied at the intersection during the injection procedure are shown as equipotential lines in Figure 2.3a and b. Both channels 2 and 3 are outlet channels and are not actively controlled. The two streams to be mixed are introduced through channels 1 and 4. The potentials of reservoirs 1 and 4 are switched to alternate between the two electric field states shown in Figure 2.3a and b. The potentials

were adjusted so that constant electric field strength was maintained downstream at outlets 2 and 3. The resulting concentration fields are shown in Figure 2.3c and d (corresponding to the electric field of Figure 2.3a) and Figure 2.3e and f (corresponding to the electric field of Figure 2.3b). Due to the symmetry that exists between the two electric fields, sample pairs are generated between channels 2 and 3 that are similar in shape, but are of the alternative solution.

Downstream of the injector shown in Figure 2.3, channels 2 and 3 are connected to a common expansion chamber with the mixed solution flowing through a single outlet channel. The integration of the dual outlet injector with the expansion region is shown in Figure 2.4. The switching of the electric field associated with the injection scheme does not produce significant fluctuations downstream in the expansion chamber. The electric field is effectively constant in this region and is of low relative strength, as shown in Figure 2.4a. Equipotential lines are relatively uniform resulting in similar fluid velocities and an even distribution of the two solutions within the expansion region. The corresponding concentration field is given in Figure 2.4b. At the exit of the expansion region, axial mixing is effectively complete; however, significant concentration gradients remain in the cross-stream direction. These cross-stream concentration gradients are caused by a bias in the injection scheme which results in an unequal delivery of the injected solutions to channels 2 and 3. The result is that one half of the expansion region becomes solution-A-rich with the other half becoming solution-A-poor.

The cause of the injection bias is shown in Figure 2.5. At the instant shown, the injection of solution B has occurred for 12ms and its leading edge has passed through the intersection into outlet channels 2 and 3. It can be seen that solution B has advanced

further into its neighbouring channel (channel 3) than it has into channel 2. The transition between the injection of each solution causes an uneven distribution at the interface between solutions A and B. The result is that channel 2 receives more of solution A ($\bar{c} > 0.5$). Conversely, in channel 3 less solution A is received ($\bar{c} < 0.5$). The transition region is approximately 2 channel widths in length regardless of the sample length, and does not change over the injection frequencies examined.

The cross-stream concentration profiles located 100μm downstream from the exit of the dual outlet sequential injection micromixer for different injection geometries and electric field switch times are shown in Figure 2.6. Three injector geometries were investigated using various injector-channel widths: a 50μm channel width cross, a 25μm channel width cross, and a hybrid cross with 50μm channels leading into the intersection and 25μm channels leading out of the intersection. In addition, separate simulations were performed with switch times of 0.2 and 0.05s on the 25μm channel width cross. In each case, the output was effectively steady-state showing negligible temporal fluctuations, however, cross-stream concentration gradients were still present in all cases. The outflow for the 50μm injector channel and a 0.2s switch time reached 68% mixed. The area at the injection cross was reduced in the cases of the 50/25μm hybrid cross and the 25μm cross. The results for these simulations, using the same switch time (0.2s), were 74.6 and 90.5% mixed respectively. The smaller channel width of the 25μm cross produced longer samples, thereby reducing the effect of the injection bias, as can be seen by the flatter concentration profile for this case in Figure 2.6 (solid line). When, the switch time was decreased to 0.05 seconds, the outflow stream was only 59% mixed. This is because the increased effect of the injection bias outweighed any axial diffusion benefits associated

with high switching frequencies and smaller injections. Thus a tradeoff exists: higher injection frequencies facilitate increased axial diffusion rates, but lower frequencies reduce cross-stream concentration gradients in the output due to injection bias. Most importantly, these results indicate that the effectiveness of this micromixing strategy is critically dependant upon the injection method employed.

2.3.4 Symmetrical Sequential Injector

Refinements were made to the dual outlet injector to reduce the cross-stream gradients caused by the injection bias. The injection bias was produced due to an asymmetry in the distribution of the two inlet solutions. This issue was resolved in the single outlet injector by creating symmetry between the inlet species across the centerline of channels 2 and 4 as shown in Figure 2.7a. Here, solution A is injected through channels 1 and 3 with solution B being injected through channel 4. In Figures 2-7b-e, the sequence is shown for one complete injection cycle with arrows indicating the direction of flow in each of the channels. During the injection of solution A, the electrical potentials are applied such that there is a small electroosmotic retraction velocity in the channel containing solution B. A similar retraction of solution A is induced during the injection of solution B. This retraction velocity ensures discrete injections with minimum leakage. As shown in Figure 2.7c, the samples produced are symmetric with respect to the channel centreline, but not uniform in the cross-stream direction. This irregularity will result in a higher normalized concentration along the upper and lower walls of the outlet channel with a lower concentration about the centerline.

The symmetrical sequential injection mixer was simulated for three sets of running conditions with the results shown in Figure 2.8. The ratio between the injection and retraction electric field strengths was adjusted while maintaining the outlet velocity condition. In test cases 1 and 2, the effect of changing the retraction electric field strength on the mixing quality was examined. For all simulations, the applied potentials were chosen so that the outlet electric field strength was maintained at 288 V/cm, corresponding to an outlet velocity of 1mm/s. All electric field strengths are specified at the intersection with towards-the-intersection being positive and all are normalized with respect to the magnitude of the output channel field strength (288V/cm). Normalized electric field strengths applied for case 1 are $E_1^* = E_3^* = 0.528$, and $E_4^* = -0.056$ for the initial step and $E_1^* = E_3^* = -0.028$, and $E_4^* = 1.056$ for the second step. Similarly in case 2, $E_1^* = E_3^* = 0.563$, and $E_4^* = -0.125$ for the initial step and $E_1^* = E_3^* = -0.073$, and $E_4^* = 1.142$ for the second step. As seen in Figure 2.8a, increasing the retraction electric field strength from case 1 to case 2 had very little effect on the streamwise mixing rate, however a significant decrease in cross-stream concentration gradients can be seen in Figure 2.8b. Increasing the retraction electric field strengths further from case 2 did not produce significant gains so this effect was not studied further. In test case 3, the effect of increasing the switch time was examined. The same electric fields were used as in case 2 but the switch time was decreased from 0.3 to 0.15 seconds. The result was significantly faster streamwise mixing as shown by the rapid decrease in concentration along the centerline plotted in Figure 2.8a; however, as shown in Figure 2.8b, significant cross-stream concentration gradients developed. This result is in keeping with that of the dual

output sequential injection micromixer, where increased injection bias effects were shown to correspond with increased switch frequency.

The cross-stream concentration gradients of case 3 were effectively eliminated by increasing the length of the injector channel by 1mm in the region between the channel cross and the rapid expansion. The injector channel width is relatively small, resulting in high concentration gradients in the cross-stream direction. The lengthened injection channel serves to rapidly reduce the cross-stream gradients at the solution interfaces prior to entering the expansion region. Using the same electric field strengths and switch time as in case 3, the outlet cross-stream concentration gradients are reduced to within +/- 1% of the perfectly mixed value of c*=0.5 while adding only 1mm to the injector channel length. The results from this case are represented by the dash-dot line in Figure 2.8b, with a corresponding concentration field plot shown in Figure 2.9. This sequential injection micromixer produces a 99% mixed solution at a flow rate of 1mm/s. The total on-chip length of the injector-expansion combination is 2.3mm and essentially all of the mixing occurs in the 1.2mm expansion chamber. In comparison, a standard 100μm wide T-mixer with a flow velocity of 1mm/s would take well over 10mm to produce a solution that is only 90% mixed and over 14mm to achieve 99% mixing. The sequential injection micromixer results are also competitive with recent mixing strategies based on patterned, non-uniform zeta potential. The heterogeneous surface charge mixer of Biddiss et al (2004) obtained 96% mixing after 1.8mm, traveling at 0.92mm/s with a diffusion coefficient of 4.37e-10m^2s^{-1}. When compared with T-mixer geometries, the sequential injection micromixer requires a larger planform area per unit length, however, this is not considered to be a major disadvantage because there is typically a significant amount of

available space located perpendicular to the channel flow direction, and axial channel length is a more critical parameter with respect to on-chip process integration.

2.4 Experimental Setup

2.4.1 Chemicals and Materials

Channel structure templates were fabricated on standard glass microscope slides by exposing photoresist SU-8 25 (MicroChem, Newton, MA) and developing with SU-8 developer (MicroChem, Newton, MA). Microchannels were formed by curing polydimethylsiloxane (PDMS) on the template, using a 10:1 base to curing agent ratio (Sylgard 184 Elastomer, Dow Corning Canada, Mississauga, ON). Sodium (bi)carbonate buffer was employed with an ionic strength I = 0.05 and pH 9.0. For fluorescent imaging, Rhodamine-B was dissolved with the buffer solution to a concentration of 0.5 mM. Rhodamine-B is neutral at pH 9.0 and exhibits a diffusion coefficient of 2.8×10^{-10} $m^2 s^{-1}$ [Culbertson et al. (1998)]. Before use, all solutions were filtered through 0.2μm pore size syringe filters.

2.4.2 Microchannel Fabrication

Microchannels were produced using established soft-lithography techniques [Duffy et al. (1998), McDonald et al. (2000)]. Photomasks of the microchip geometry were drafted and then printed using a high-resolution commercial image setter (Island Graphics, Victoria, BC) from the EPS file format. Microscope slides were soaked in acetone for several hours, dried, and exposed to oxygen plasma for one minute prior to coating in order to improve surface cleanliness and promote adhesion of the photoresist.

A layer of SU-8 photoresist was applied to the surface of the slide and spun at a speed of 3000 rpm for 45 seconds, resulting in a thickness of 16μm. The coated slides were pre-baked at 65°C for five minutes and at 95°C for 15 minutes to harden. The photomask was positioned on the slide and exposed under a collimated UV light source for 30 seconds. Polymerization was promoted by post-exposure baking at 65°C for one minute followed by five minutes at 95°C. The exposed slides were then developed for approximately two minutes to remove all unexposed photoresist, creating negative templates. Channels were formed by curing a 2mm thick layer of PDMS on the templates at 70°C for three hours at a pressure of –86 kPa. The PDMS structure was irreversibly sealed to a clean glass slide to complete the channel structure after both surfaces were exposed briefly to oxygen plasma.

2.4.3 Electric Field Control

Discrete samples were produced in the symmetrical sequential microfluidic mixer by switching the electric field between two predefined states, resulting in a corresponding change in electroosmotic velocity. The rate at which the electric fields change is termed the switch frequency (f_s) and is actively controlled using Labview software and a high voltage switching device. A high voltage power supply was connected to a series of adjustable potential dividers which were used to produce the four required operating potentials. These potentials were divided into two pairs and connected to the inputs of the relay. The voltage outputs from the relay were then connected to reservoirs A and B of the microfluidic chip.

2.4.4 Data Collection and Image Processing

The Rhodamine-B and buffer solutions were introduced to the two upstream reservoirs (A and B) of the micromixer. Fluid transport was observed using a Leica DM LM fluorescence microscope with 5x and 10x objectives. Illumination was supplied by a mercury arc lamp. Still images of the operating micromixer were acquired using a Retiga 1300i FAST 1394 12-bit digital camera and QCapture Pro software package, with an exposure time of 5 milliseconds. The acquired images had a resolution of 515 x 650 pixels. Images were exported in TIF format to MATLAB for post-processing. Images were normalized by subtracting a dark-field image and scaling against a bright field image. Concentration profiles were created by individual pixel intensity values taken from the normalized images and scaled to fill the output range. The resulting normalized concentrations of 1 and 0 represent the unmixed concentrations of solutions of A and B respectively.

2.5 Experimental Results and Discussion

Both a schematic and magnified view of the micromixer in operation are shown in Figure 2.10. To ensure symmetric operation, and keep the number of reservoirs and associated infrastructure to a minimum, both the injection channels containing solution B are looped back and connected to a common reservoir. Near the intersection, the three inlet channels are narrowed from 100μm wide to 50μm to reduce the dead-volume in the intersection and locally concentrate the electric field. The expansion chamber is 1.2mm long end-to-end with 45° expansion angles and a 100μm wide outlet channel. The height

of the channel structure is uniformly 16μm. During operation, solutions A and B are injected sequentially into the intersection by switching of the voltages applied to reservoirs A and B via platinum electrodes. The downstream reservoir voltage was maintained at ground. The voltage applied at each electrode in each state, and the switch frequency was controlled through Labview software, the data input/output board and the high voltage switching device.

A complete cycle of the injection process is shown for a 1 Hz switch frequency in Figure 2.11. For the injection of solution A, electric potentials of 940V and 670V were applied at reservoirs A and B respectively. Similarly for the injection of solution B, electric potentials of 630V and 806V were applied to reservoirs A and B respectively. In Figure 2.11a, the injection of solution A has been initiated. The electric fields were chosen such that a small retraction velocity is produced in the vertical channels (Figure 2.11b). Similar to the pull-back voltage applied in pinched injection schemes [Ermakov et al. (2000)], the retraction voltage was found to increase the quality of the injected samples by reducing leakage. The length of the produced sample is proportional to the outlet stream velocity and inversely proportional to the switch frequency. After a switch of the electric field the injection of solution B is initiated (Figure 2.11c). Again, a small retraction voltage is employed to ensure that a discrete injection is produced with minimal leakage at the intersection. This sequence is then repeated indefinitely, producing a series of sequential samples flowing at constant velocity through the outlet channel. As shown in Figure 2.11d, the samples produced are symmetric with respect to the horizontal channel centreline; however, they are not entirely uniform in the cross-stream direction. It was found through the numerical investigation (Section 2.3.4) that if

this cross-sectional concentration gradient is not sufficiently diffused prior to entering the expansion chamber, significant lingering cross-stream gradients will result. Specifically, solution A will have a lower mean concentration along the outside of the outlet channel and a higher mean concentration along the centerline, in agreement with the numerical results. A 1mm channel length (as shown in Figure 2.10, inset) connecting the injector from the expansion chamber facilitated rapid cross-stream diffusion to reduce these cross-stream gradients.

From the connecting channel to the expansion region, the axial velocity reduces from 2 mm/s to 0.1 mm/s. This corresponds to a decrease in Reynolds number from Re = 0.05 to Re = 0.003, and a 400-fold decrease in Peclet number from Pe = 7100 to Pe = 18 for the 1 Hz switch frequency case. Switch frequencies of 0.5Hz, 1Hz, 2Hz, 5Hz, and 10Hz were studied while maintaining the applied fields as employed previously. Figure 2.12 shows the measured normalized concentration fields in the expansion region for each frequency tested. The concentration field in Figure 2.12a shows that significant axial concentration gradients remain at the outlet, indicating that a switch frequency of 0.5Hz is not high enough to achieve efficient mixing and will result in concentration fluctuations at the outlet. As the switch frequency is increased to 1 Hz, 2Hz, 5Hz and 10Hz (Figure 2.12b,c,d,e), axial concentration gradients are reduced sooner and fluctuations in the output are eliminated.

Figure 2.13 facilitates a more quantitative analysis of the field data presented in Figure 2.12. For each frequency, axial concentration profiles are plotted along the channel centerline in Figure 2.13a, and cross-stream concentration profiles are plotted at the mixer outlet (100μm downstream of the contraction) in Figure 2.13b. Spatial and

temporal oscillations in the concentration field are apparent, particularly at the expansion entrance and for the low frequency cases. These oscillations quickly decrease in magnitude through the expansion region due to the locally decreased Peclet number. At the lowest frequency tested (0.5 Hz), spatial and temporal fluctuations remain present in the outlet stream (also apparent in Figure 2.12a). The outlet cross-stream profiles obtained for 1 and 2 Hz exhibit negligible cross-stream gradients, are effectively indistinguishable, and were constant over time indicating that highly efficient mixing was achieved at these frequencies. At the higher frequencies (5 and 10 Hz), although temporal variations are quickly diminished, the mixed concentration of the outlet stream is observed to increase with the switch frequency. It is expected that this dependence on frequency is a result of the injection process. Specifically at higher frequencies, the final concentration of the mixed output is dependant on both the switch frequency and the applied electric fields. For the chip geometry and flow rate studied here, 1-2 Hz has been observed as the preferred operating range. At these frequencies a steady output of 99% mixed solution was achieved. This degree of mixing is 'complete' in the context of the expected imaging error, which is on the order of ±1% of full scale (as discussed in section 1.3.3.4)

It was found that the production of a wide range of solution concentrations can be obtained using the same mixer geometry and electric fields, while changing the duty cycle of the switch frequency. The duty cycle (*dc*) is defined as the following:

$$dc = \frac{T_A}{T_A + T_B} = T_A \times f_s \qquad (2.4)$$

where T_A and T_B are the period of time that the electric field of state A and state B are on during an injection cycle respectively, and f_s is the switch frequency. For example, a duty cycle of 0.5 implies that the electric field of state A and state B are left on for equal amounts of time, whereas a duty cycle of 0.75 implies that the electric field of state A is on for 75% of each injection cycle. Results for the various duty cycles employed can be seen for a 1 Hz switch frequency in Figure 2.14. Axial concentration profiles are plotted along the centerline of the expansion region in Figure 2.14a for duty cycle values of 0.3, 0.4, 0.5, 0.7 and 0.9. The electric fields were adjusted such that the normalized concentration at the outlet was equal to c* = 0.5 for the 0.5 duty cycle case and the outlet velocity was constant at $1 mms^{-1}$. As expected, the normalized outlet concentration varied with the duty cycle. The large range of accessible outlet concentrations is noteworthy. The results show that the relationship between outlet concentration and duty cycle is not perfectly linear. This non-linearity is a function of the injection process and the electric fields employed. In practice, both the electric field and the duty cycle must be considered in 'tuning' of the output. Shown inset in Figure 2.14a are the concentration fields for the 0.9, 0.5 and 0.3 duty cycle cases. In Figure 2.14b, cross-stream concentration profiles are shown for the entire range of duty cycles taken in the outlet channel, 100μm downstream from the contraction. The results indicate that by varying only the operating parameters, this microfluidic mixer can produce a uniformly mixed solution at virtually any desired outlet concentration.

2.6 Summary

In this work, a novel micromixing strategy was developed and tested both numerically and experimentally. The numerical investigation demonstrated the axial diffusion of a continuous sequence of discrete samples in a microchannel expansion. The mixing of a continuous sequence in a sudden expansion region was first characterized assuming an ideal, square-wave injection input. Different expansion geometries were examined as well as different injection frequencies. Increasing injection frequency was found to greatly increase the effectiveness of the mixer. To incorporate this mixing strategy on-chip, two new injection schemes were developed which are feasible for on-chip integration. Both integrated micromixer designs demonstrate rapid axial mixing of the individual stream sequences. For the dual outlet mixer, cross-stream gradients in the output channel developed due to an inherent bias in the injection technique. These results indicate that the effectiveness of this micromixing strategy is critically dependant upon the injection method. It was found that the benefit associated with higher switching frequencies (i.e. smaller samples) can be outweighed by the effect of increased injection bias in this micromixer. The injection bias was reduced, but not eliminated, by decreasing the width of the channels at the injection cross and increasing the sample length. Using a symmetrical sequential injector design and an increased injection channel length, cross-stream concentration gradients were effectively eliminated. These numerical results indicate that the sequential injection micromixer has the potential to produce a 99% mixed solution at a flow rate of 1mm/s in only 2.3mm.

The symmetric sequential injector was then tested experimentally using fluorescence microscopy. It was found that for injection frequencies in the range of 1-2Hz

the final mixed concentration value was only a function of the applied potentials and not the switch frequency. At lower frequencies (0.5Hz), mixing was incomplete, exhibiting spatial and temporal variations in concentration at the outlet. At frequencies above the preferred operating range, the outlet concentration becomes dependant on injection frequency. In general, the preferred operating frequency will be a function of both the chip geometry and flow rate required. The later is ultimately determined by the application. In addition, the duty cycle of the injection signal was modified through values of 0.3 – 0.9. It was observed that outlet concentrations can be easily modified using this method. By varying only the operating parameters, this microfluidic mixer can produce a uniformly mixed solution at virtually any desired outlet concentration.

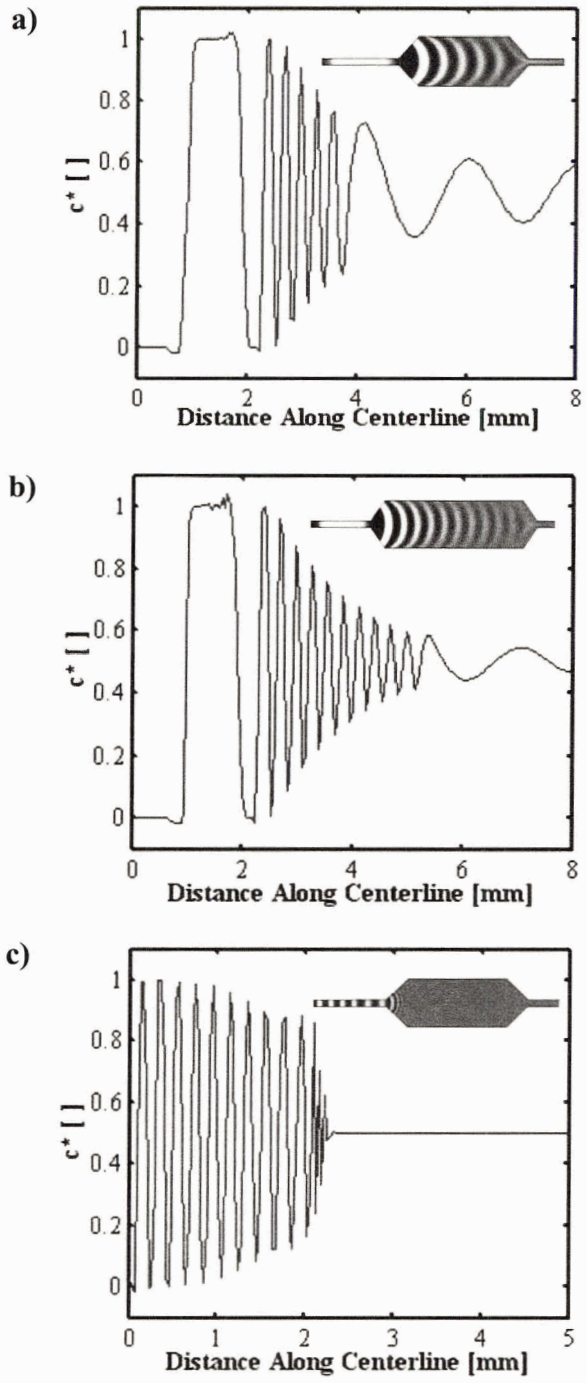

Figure 2.1 Axial concentration profiles plotted along the channel centerline with 2-D concentration fields shown inset. (a) 2mm expansion with 1mm sample length, (b) 5.5mm expansion with 1mm sample length, (c) 2mm expansion with 100μm sample length. [Numerical]

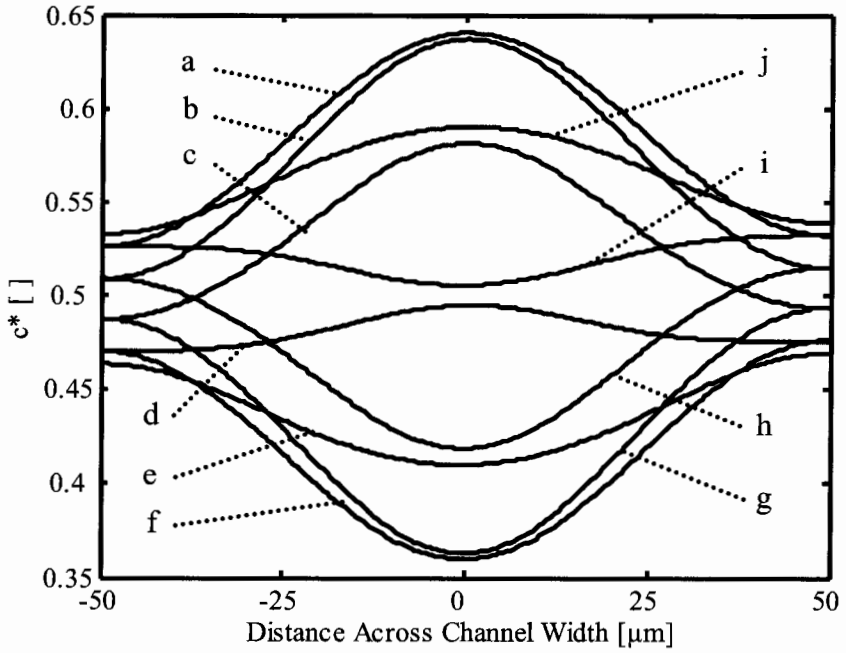

Figure 2.2 Cross-stream concentration profiles taken 100μm downstream from the exit of the 2mm expansion in Fig. 1a. The profiles are plotted for 10 equal time intervals (a → j) over the two second injection period (1mm samples, 1mm/s). [Numerical]

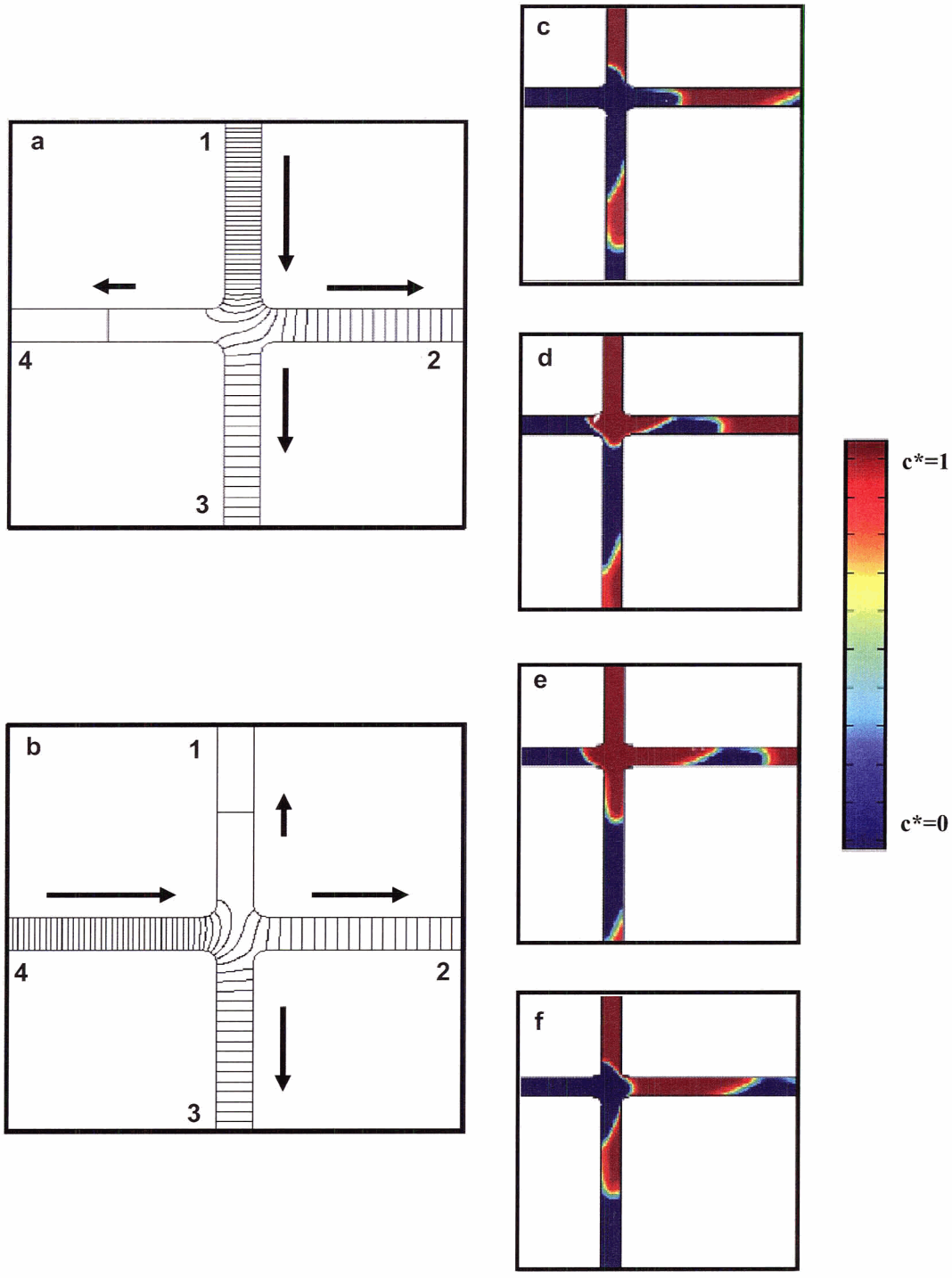

Figure 2.3 Operation of the sequential sample injector. Equipotential lines are presented for the two electric field states (a) and (b). Arrows indicate the direction and relative magnitude of the induced fluid velocity. The resulting concentration profiles for a 0.3s injection cycle are shown at equal time intervals of 75ms in (c)→(f) . [Numerical]

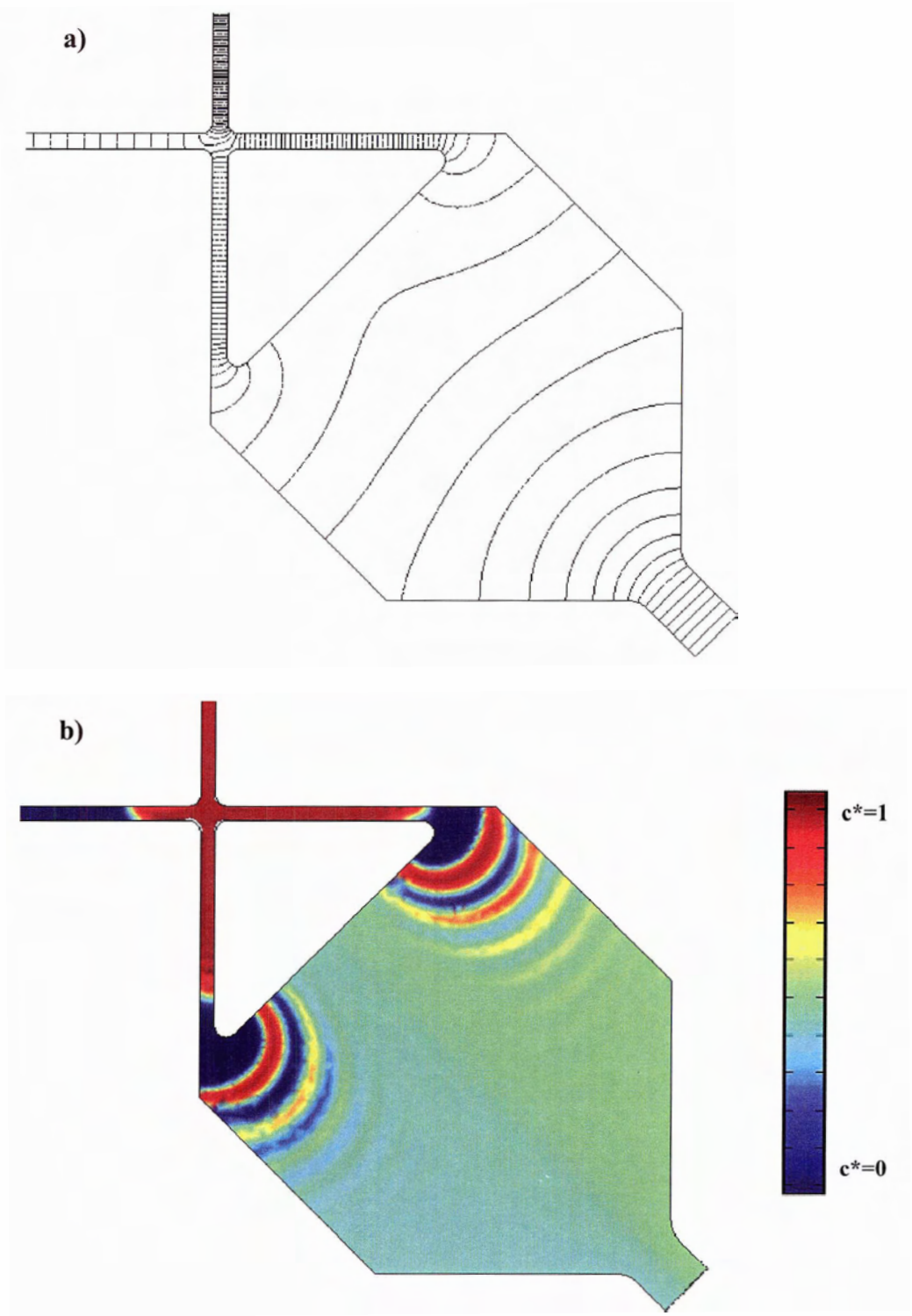

Figure 2.4 Simulation results for (a) equipotential lines and (b) the concentration profile for the dual outlet sequential injection micromixer. [Numerical]

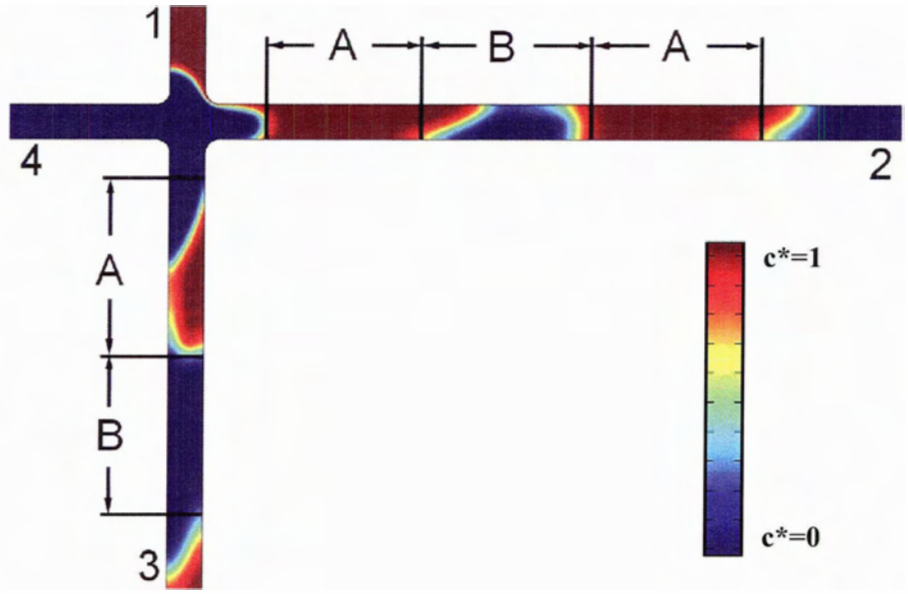

Figure 2.5 Concentration profiles showing the cause of the injection bias for 25μm channels with 0.05s switch time. In channel 2, Region A is purely solution A but Region B is comprised of both solutions A and B due to the flow lag though the intersection. The result is that the outflow of channel 2 is solution-A-rich and channel 3 is solution-A-poor. [Numerical]

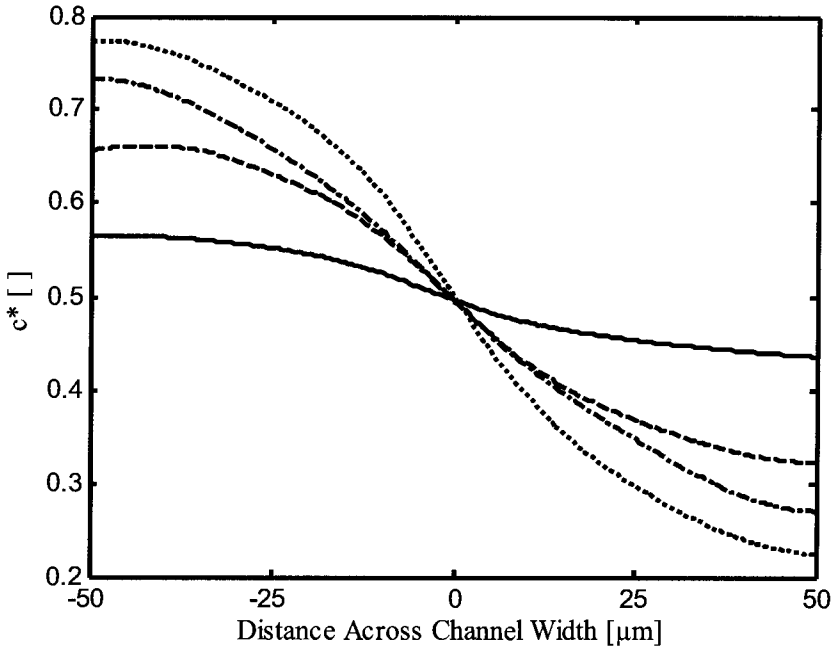

Figure 2.6 Cross-stream concentration profiles taken 100μm downstream from the exit of the sequential sample micromixer for a 0.2s switch time with channel widths of 50μm (dash-dot), 25μm (solid), and 50/25μm hybrid (dash). Also, results for the 0.05s switch time with the 25μm channel width cross (dot) are shown. [Numerical]

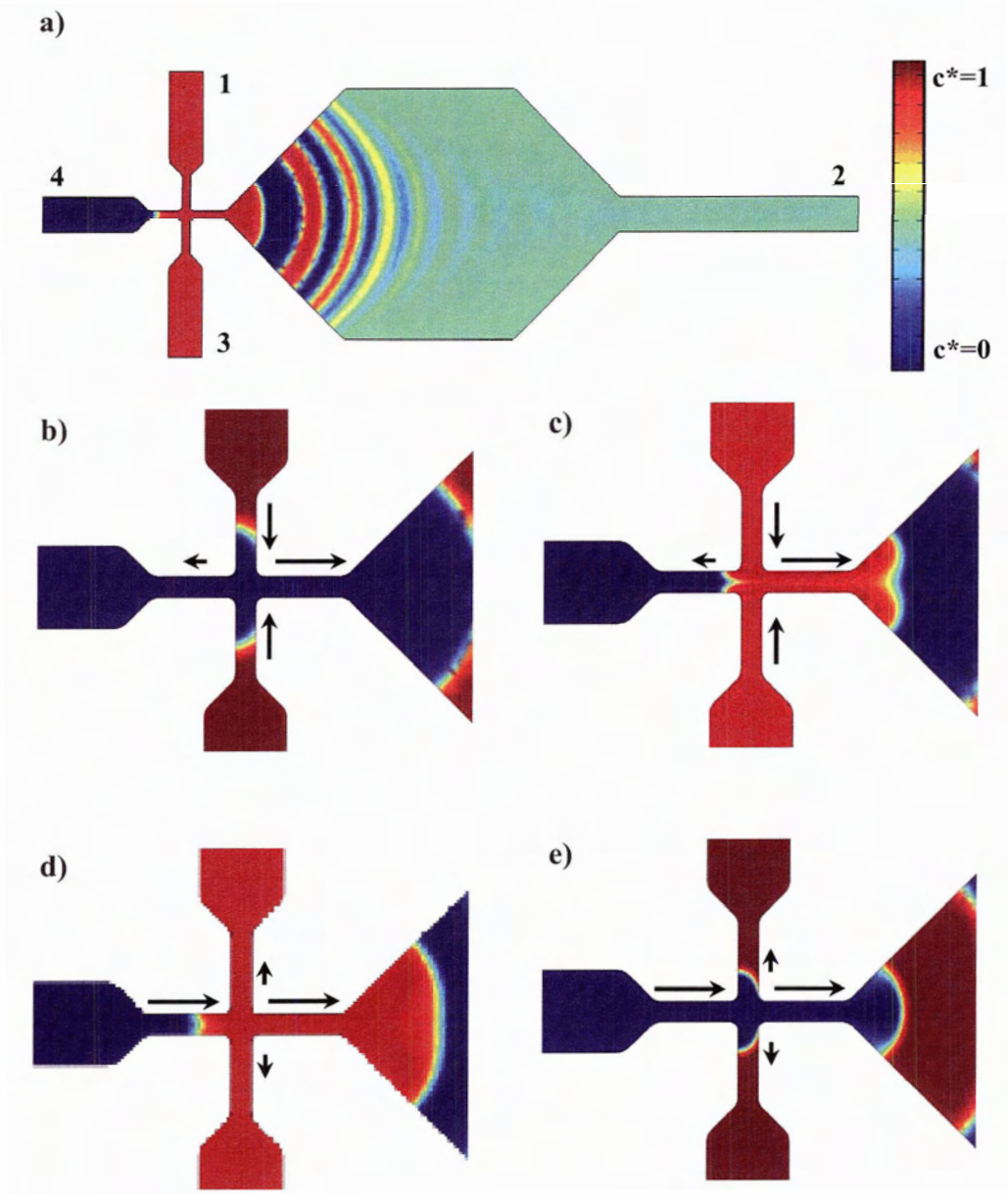

Figure 2.7 The concentration field for the symmetrical sequential injection micromixer is shown in a). The sequence for a 0.6s injection cycle is shown at equal increments of 0.15s in b) → e). [Numerical]

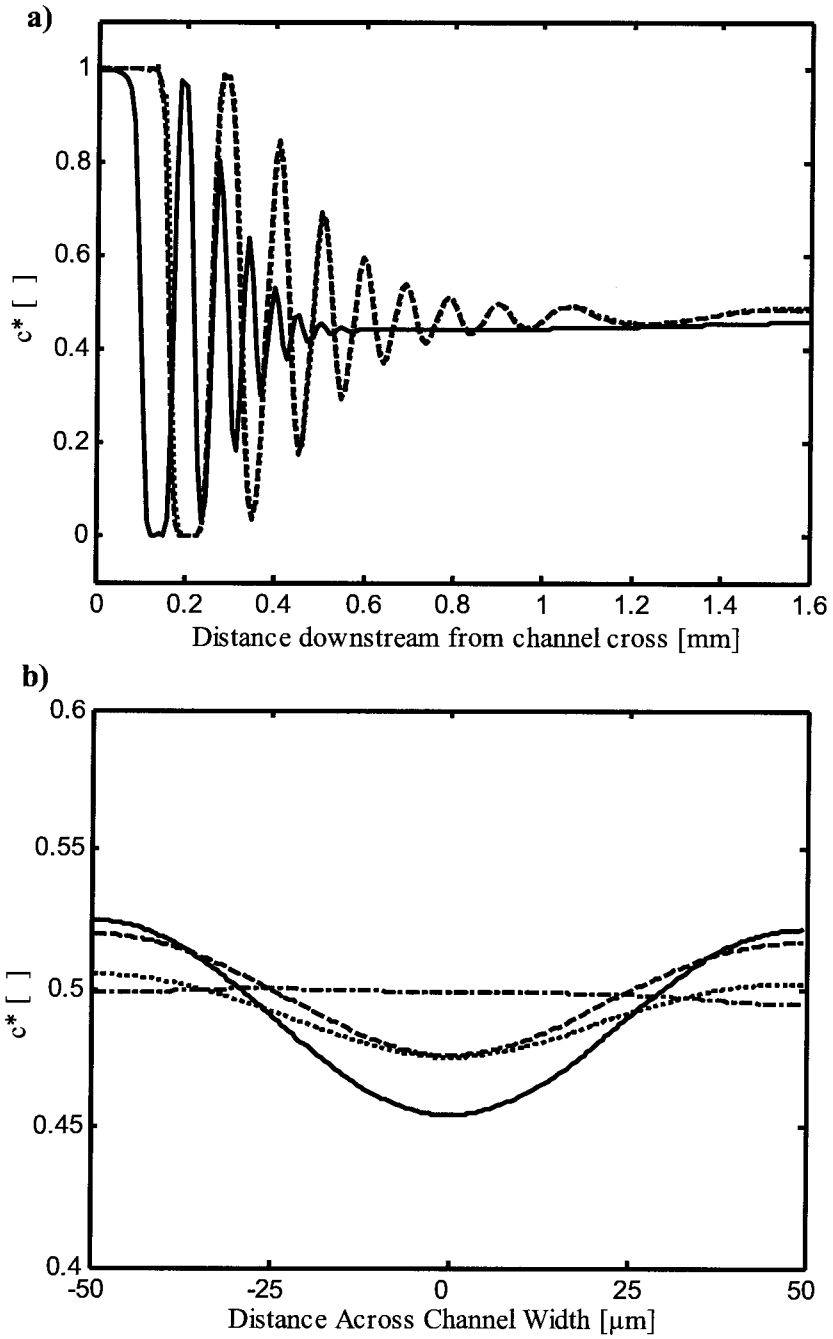

Figure 2.8 Axial concentration profiles are plotted along the centerline in (a) and cross-stream concentration profiles at the exit of the expansion region are plotted in (b). Results for case 1 (dash), case 2 (dot), case 3 (solid) are presented; however, cases 1 and 2 are indistinguishable in (a). Additionally, the cross-stream concentration profile for case 3 with the lengthened injection channel is shown (dash-dot) in (b). [Numerical]

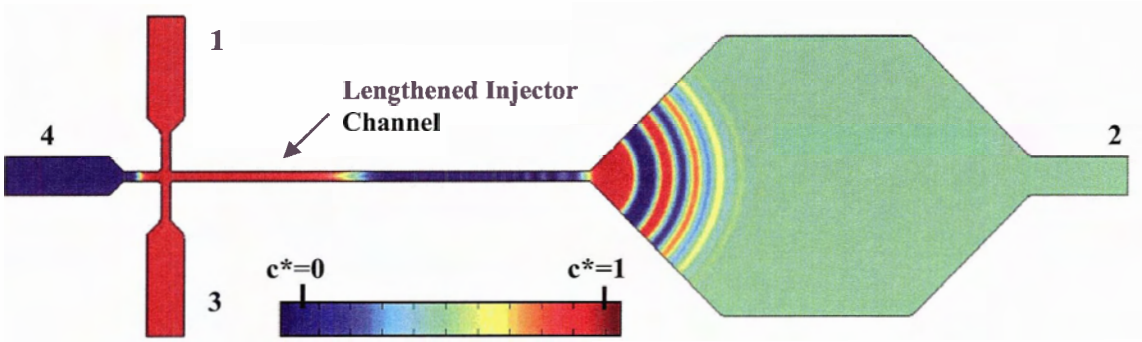

Figure 2.9 Concentration field for the symmetrical sequential injection scheme with a lengthened injection outlet channel. Outlet cross-stream gradients are effectively eliminated using the longer injection channel which reduces cross-stream gradients at the solution interfaces prior to expansion. The output is 99% mixed within a length of 2.3mm. [Numerical]

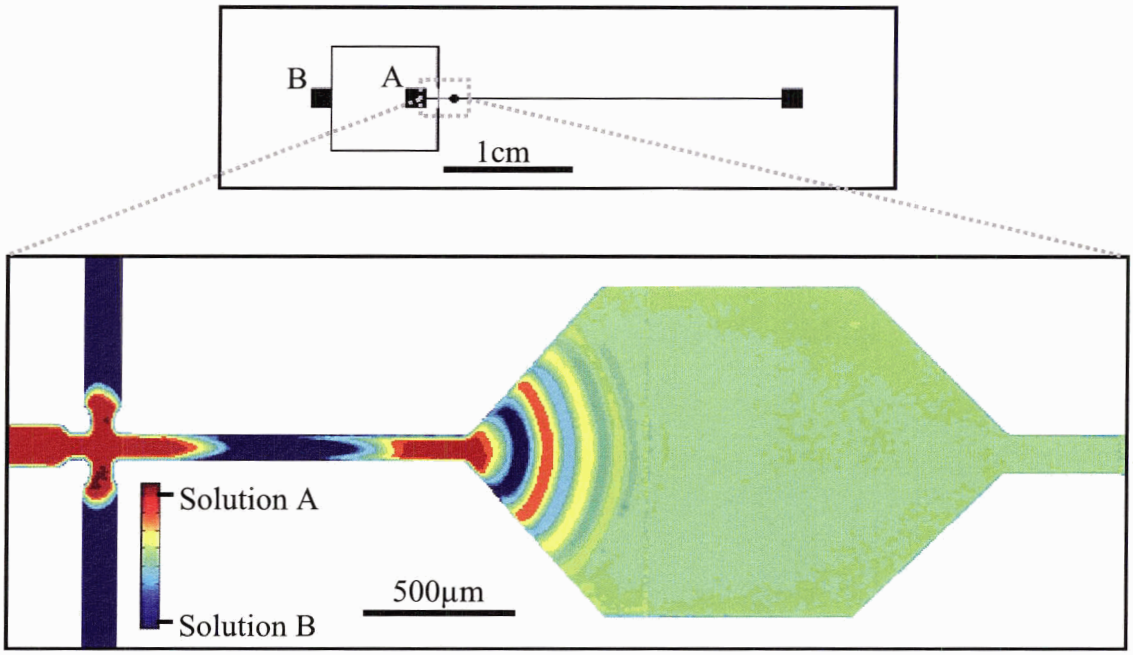

Figure 2.10 Top, a schematic of the on-chip layout of the symmetrical sequential injection micromixer. Bottom, a magnified view of the micromixer in operation. [Experimental]

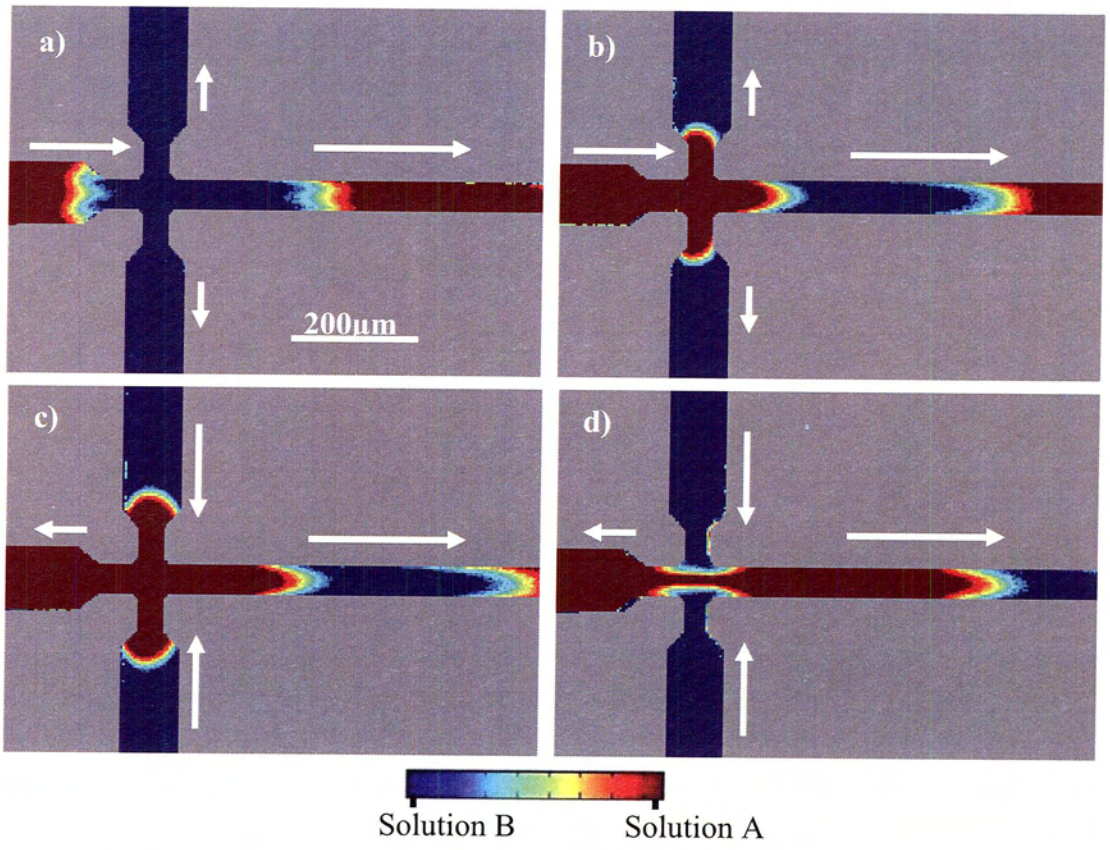

Figure 2.11 Concentration fields are shown for one complete injection cycle (1s) operating with a switch frequency of 1 Hz (a) → (d). Arrows indicate the relative magnitude and direction of the velocity field. [Experimental]

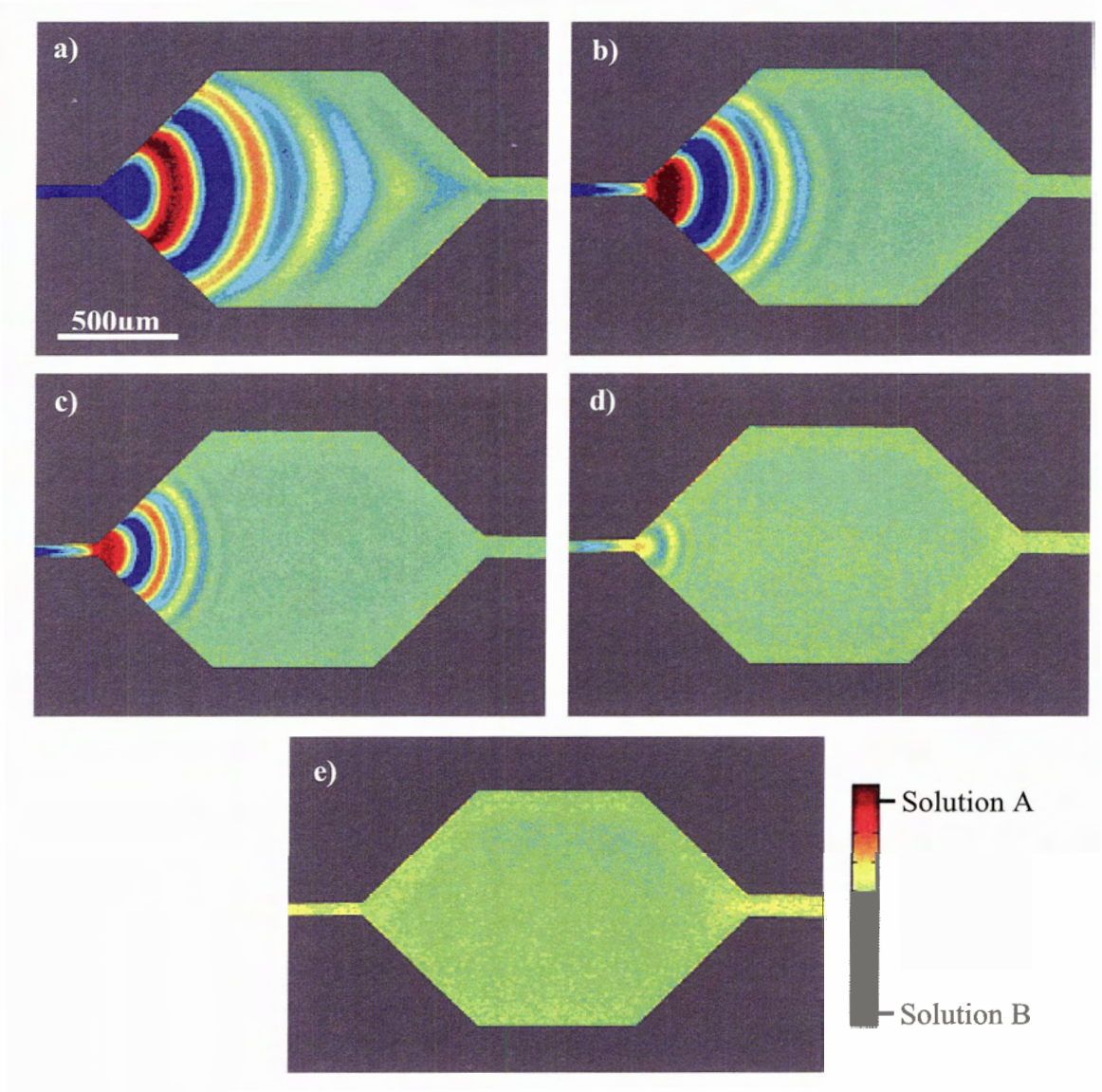

Figure 2.12 Concentration fields are shown for the expansion region for switch frequencies of a) 0.5Hz, b) 1Hz, c) 2Hz, d) 5Hz, and e) 10Hz. [Experimental]

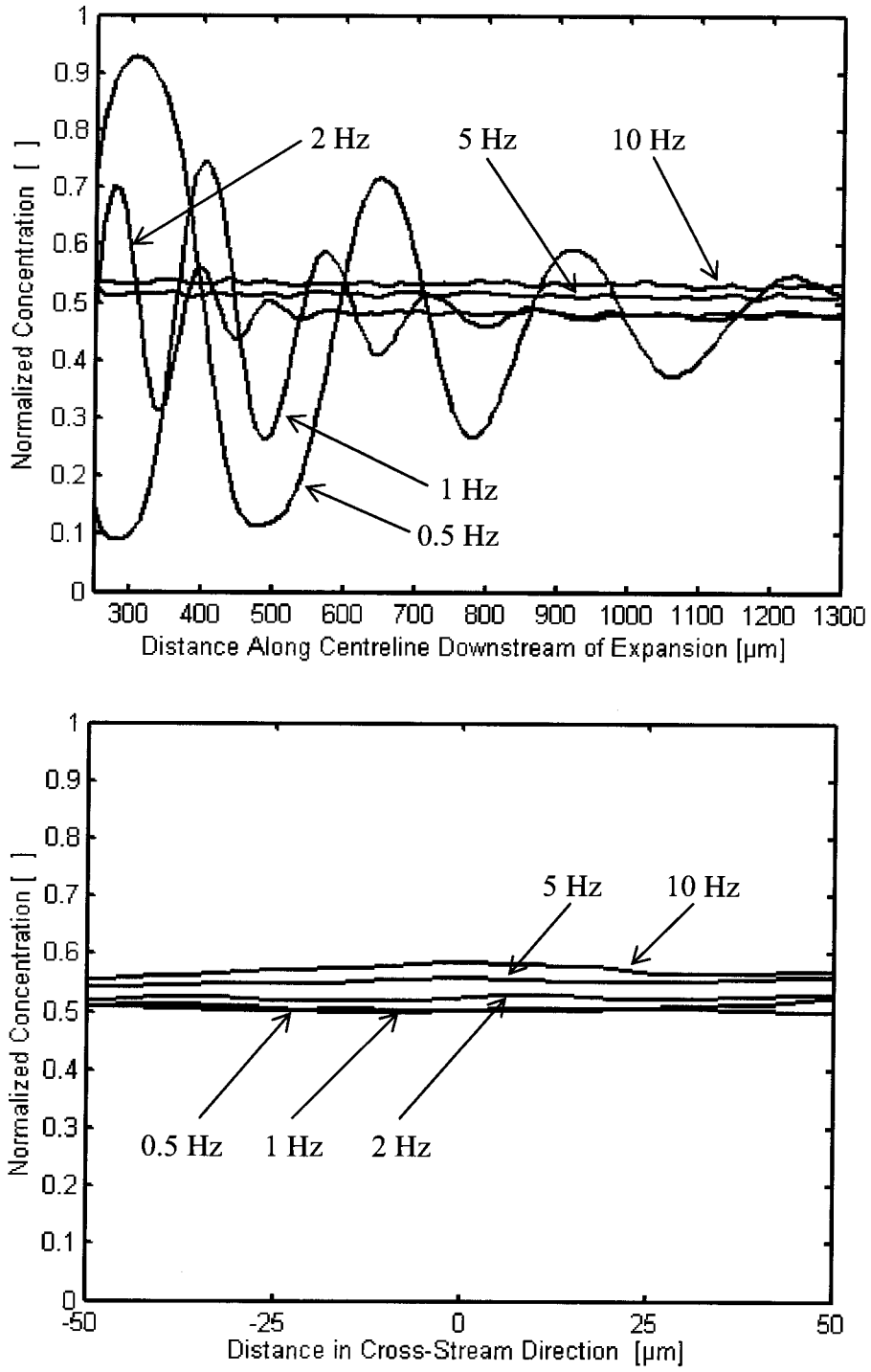

Figure 2.13 Axial concentration profiles are plotted along the centerline (a) and cross-sectional concentration profiles plotted across the mixer outlet (100μm downstream from the contraction) (b) for the labeled switch frequencies. [Experimental]

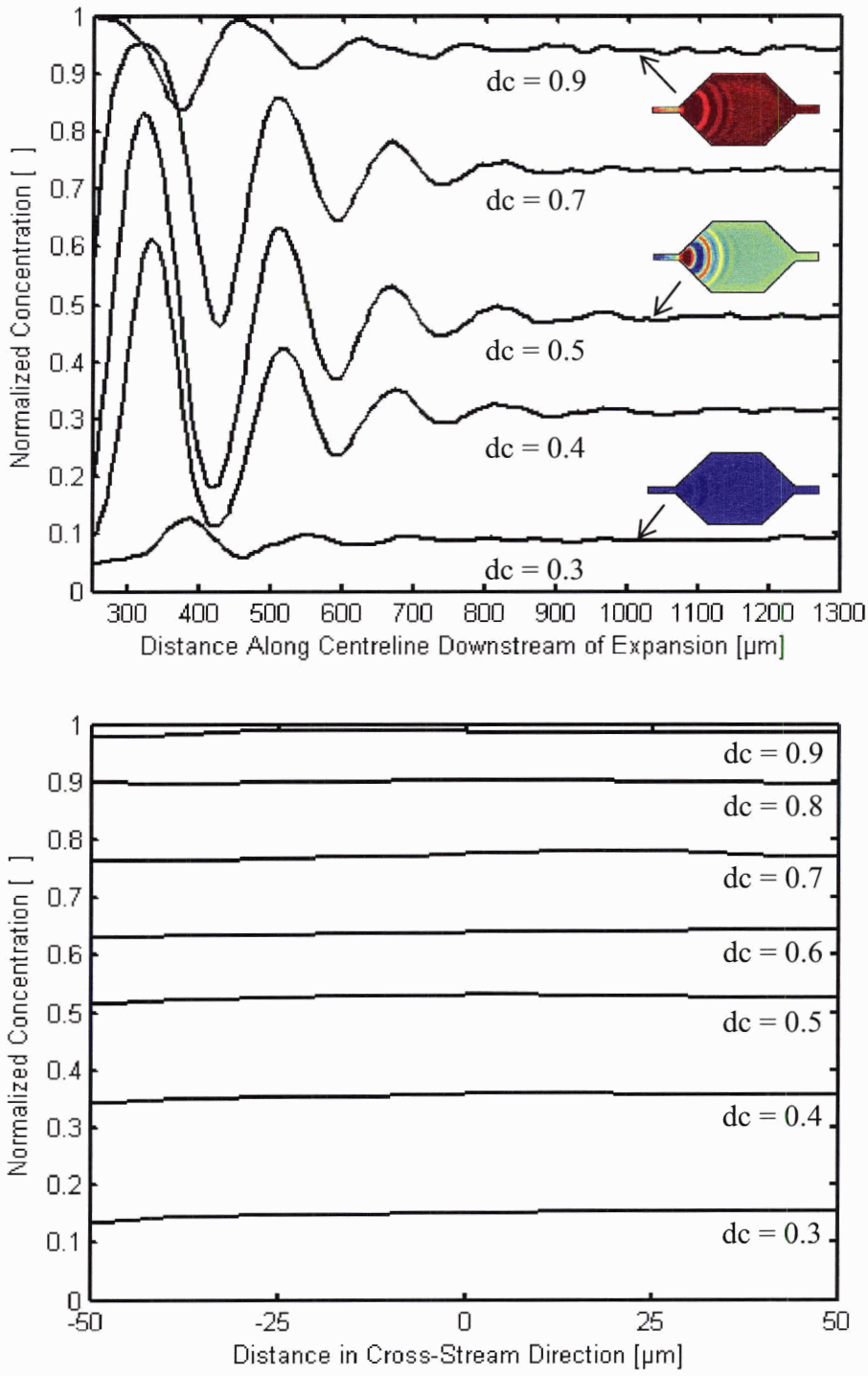

Figure 2.14 Axial concentration profiles are plotted along the centerline (a) and cross-sectional concentration profiles plotted across the mixer outlet (100μm downstream from the contraction) (b) for 1Hz switch frequency with duty cycle shown at right. Concentration fields are shown inset (a) for duty cycles of 0.9, 0.5 and 0.3 (top to bottom). [Experimental]

Chapter 3

THREE-DIMENSIONAL MICROFLUIDIC FOCUSING USING STRATEGIC SURFACE CHARGE PATTERNING

In this chapter, a strategy is developed for three-dimensional hydrodynamic focusing on a planar microfluidic chip. Numerical simulations demonstrate that depthwise focusing can be achieved through the use of strategically-patterned surface charge. In-plane hydrodynamic focusing first is achieved using a sheath fluid and a microfluidic cross geometry. The addition of depthwise focusing is examined using two different surface charge configurations: a structure with top surface patch, and a structure with both top and bottom surface patches.

3.1 Background

3.1.1 Surface Charge Treatment

The electrical double layer, which is the basis for electrokinetic phenomena, forms in response to interfacial surface charge. Non-uniformities in surface charge result in a non-uniform zeta-potential distribution. In such cases, non-uniform electroosmotic

wall velocities develop when an axial electric field is applied. Non-uniformities in zeta-potential commonly occur in hybrid microfluidic systems made up of different materials. The most common example is the combination of a replica-molded polydimethylsiloxane, PDMS, channel structure bonded to a glass substrate. Using glass as a base substrate provides both structural rigidity and rapid dissipation of Joule heat [Erickson et al. (2003b)]. However, the differential electroosmotic velocities developed in hybrid chips lead to increased axial dispersion of analytes, which can decrease separation efficiencies in electrokinetic separation applications [Kirby and Hasselbrink (2004a,b)].

The negative surface charge gained by PDMS upon exposure to oxygen plasma is unstable and will decay over time. The surface charge can be made more stable by coating the surfaces with ionic-polymer layers [Katayama et al. (1998a,b), Liu et al. (2000)]. When a positive ionic polymer is used, it will be immobilized against the negatively charged inner surface of a microchannel, thus changing the sign of the surface charge to positive. The surface can then be coated again with a negatively charged polymer. If left with the positive charge, however, electroosmotic flow with travel in the opposite direction (i.e. cathode to anode) under an applied electric field. This effect is shown in the schematic in Figure 3.1. In Figure 3.1a, a typical electroosmotic flow is shown for a negatively charged surface, whereas in Figure 3.1b, the surface has been coated with a positive ionic polymer and the flow direction has been reversed. When the microchannel surface is treated with a localized patch, the resulting heterogeneous surface charge distribution has been shown to induce local circulations in electroosmotic flows [Kirby and Hasselbrink (2004a,b), Stone et al. (2004)]. Most notably, these

circulations have been applied to increase stream-stream mixing in microchannels [Erickson and Li (2002), Stone et al. (2004), Biddiss et al. (2004)]. The multidirectional nature of these flows results in rapid folding of the fluid streams and greatly increased interfacial area available for diffusion.

3.1.2 Micro-Flow Cytometry

Flow cytometry involves the use of a focused laser projected through a liquid stream that contains cells, or other particles. The cells are usually stained with fluorescent dyes which bind specifically to cellular constituents, or may dye the entire cell. The dyes are excited by the laser beam, and emit a signal of light at a Stokes-shifted wavelength [Haugland (1994)]. The signal can provide information about various cellular properties based upon the intensity and wavelength of the light. A schematic of a cell sorter is shown in Figure 3.2.

Flow cytometry is used widely for biological research and for clinical diagnostics [Shapiro (2003), Weaver (2000)]. However, conventional flow cytometry devices are large and very expensive. The recent increase in microfluidic technologies shows promise for micro-sized flow cytometry devices as they can be made to be more portable and much less expensive [Yang et al. (2005), Sundararajan et al. (2004), Goranovic et al. (2001), Schrum et al. (1999), Fu et al. (1999), Chou et al. (1999)]. For proper measurements it is required that cells pass by the laser beam in single file, which requires three-dimensional hydrodynamic focusing of the sample stream. Focusing is achieved in microfluidic chips by the lamination of the sample stream with sheathing fluid streams. Two-dimensional focusing is achieved by combining a central sample stream with a

buffer sheathing flow on either side in a planar microfluidic cross geometry. This method of on-chip hydrodynamic focusing is the most common, perhaps due to the relative ease and popularity of planar microfluidic chip fabrication methods.

Hydrodynamic focusing has been used in the development of micro-flow cytometry devices with good results [Schrum et al. (1999), Fu et al. (1999), Chou et al. (1999)], however no depthwise focusing was performed in these cases. Three-dimensional on-chip focusing is desirable both for increased focus intensity, and to minimize interaction between the sample and the channel walls (many biological analytes can adhere to channel walls and mitigate optical measurements). In addition, having the sample in the centre of the channel is desirable, as fluctuations in the depthwise location of the sample will change the fluorescent signal [Lin and Lee (2003)]. Recent efforts towards three-dimensional hydrodynamic focusing on-chip have utilized multi-layer microfabrication techniques to facilitate additional out-of-plane sheathing fluid streams [Sundararajan et al. (2004), Goranovic et al. (2001), Yang et al. (2005)]. Others have taken advantage of the electric charge that can be found on cells and achieve three-dimensional focusing using dielectrophoretic forces [Lin et al. (2004b)].

3.2 Numerical Model

The model presented here was implemented in two dimensions using FEMLAB. The electric field and flow field equations are solved at steady-state using the direct (SPOOLES) solver. Care was taken during mesh generation to ensure that proper mesh refinements were made in high gradient regions according to the mesh analysis performed in section 1.3.1.2. For the electric field boundary conditions, potentials were assigned at the channel inlets, electrical ground was assigned at the outlet and zero flux

was assigned at the walls. Potentials were assigned such that the outlet velocity was constant for all cases at 1mm/s. The boundary conditions for the flow field were zero pressure at the inlet and outlet with a wall velocity boundary condition applied using the Helmholtz-Smoluchowski equation (Equation 1.2). It is noteworthy that the velocity and electric fields are not mathematically similar in this case because the zeta potential distribution is non-uniform. Finally for species transport, zero flux was imposed at the walls, a constant concentration was imposed at the inlets and a convective-only flux boundary condition was applied at the outlet. The physical properties of the solutions were taken to be those of water. A diffusion coefficient of $D = 1\text{x}10^{-10}$ m^2s^{-1} was assigned and an electroosmotic mobility of $3.5\text{x}10^{-8}$ $m^2V^{-1}s^{-1}$ was applied at native surfaces and $-3.5\text{x}10^{-8}$ $m^2V^{-1}s^{-1}$ at surface patches (corresponding to zeta potential values of ζ_o = -50mV and ζ_o = +50mV, respectively).

3.3 Results and Discussion

A three-dimensional model was applied to demonstrate that three-dimensional hydrodynamic focusing can be achieved in a planar microfluidic cross-chip architecture using strategically patterned surface charge. A microfluidic cross geometry is used with 100μm by 100μm channels. The computational domain is shown in Figure 3.3. Three separate focusing cases are presented, each driven electrokinetically with the same applied electric field. The three focusing cases are plotted in Figure 3.4, with cross-sectional concentration fields plotted at nine 100μm intervals along the central channel. Results for conventional two-dimensional focusing, with homogeneous surface charge, are plotted in Figure 3.4a. As expected, the stream is effectively focused in the plane of

the chip and no focusing occurs in the depthwise direction. The focusing achieved in Figure 3.4b results from the placement of a surface patch on the upper surface of the central channel. The patch extends across the 100μm channel width, and is 400μm in length extending 200μm upstream and 200μm downstream of the intersection. The third focusing configuration, shown in Figure 3.4c, involves an additional surface patch on the floor of the channel, directly opposite the top patch. The three-dimensional focusing is achieved due to the reversed electroosmotic velocity induced by both top and bottom surface patches. The flow circulations induced by these surface patch configurations can be seen in Figure 3.5, where streamlines are shown along the central plane of the surface patch location. It is noteworthy that the circulation region that vertically confines the flow in the central channel is comprised almost entirely of the sheath fluid. This is because the incoming sheath flow is partially entrained into the circulation zone as it enters the intersection, and thus the two focusing mechanisms work in concert. In Figure 3.6, concentration profiles are shown in the outlet channel at a location 200μm downstream of the intersection. The heterogeneous surface charge case is shown in Figure 3.6a, where the sample stream has been confined to 17% of the outlet channel. The addition of the upper surface patch (Figure 3.6b) increased the focusing of the sample stream, confining it to only 13% of the outlet area. This configuration achieves strong three-dimensional focusing using only one surface patch. Fabricating the one-patch chip is straightforward using conventional soft-lithographic microfabrication, and patch-wise surface pre-treatment of a base substrate. The focused stream, however, remains in contact with the lower surface, and thus this design would be somewhat susceptible to analyte-wall adhesion (bio-fouling). In Figure 3.6c, the upper and lower surface patch configuration is

shown to reduce the sample area to 12% of the outlet channel. Although the additional reduction in sample area is minimal, the two surface patch configuration is much more advantageous in flow cytometry applications where analyte-wall interactions may be of concern. The sample stream is not in contact with the channel walls at the interrogation region which will minimize the potential for adsorption of analytes to the microchannel surfaces.

3.4 Summary

A novel three-dimensional microfluidic focusing strategy was developed. A three dimensional numerical model was applied to demonstrate that steady-state three-dimensional hydrodynamic stream focusing can be achieved in a planar microfluidic cross-chip architecture using strategically-patterned surface charge. Configurations with one and two surface patches were found to achieve a high degree of focusing in the vertical direction, while effectively maintaining the horizontal focusing accomplished by the sheath flows. The microfluidic streams were focused to 13% and 12% of their original cross-sectional areas for the cases of one and two surface patches, respectively. The focusing was most effective due to the circulation zone entraining the sheath solution from the side channels. The two patch design has the added benefit that the sample stream is focused to the centre of the microchannel and has minimal contact with the microchannel walls in the detection region; an important consideration for some readily adsorbed biological analytes.

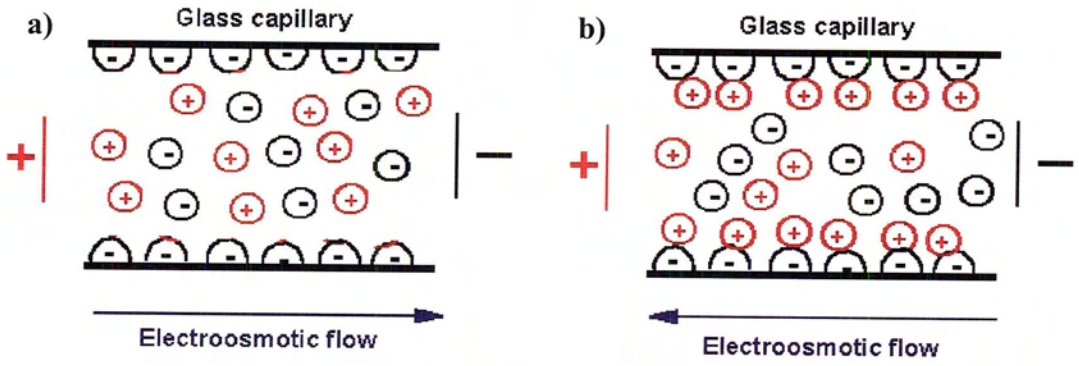

Figure 3.1 The effect of surface treatment on the direction of electroosmotic flow is shown for a negative native surface charge (a) and the positively coated surface (b).

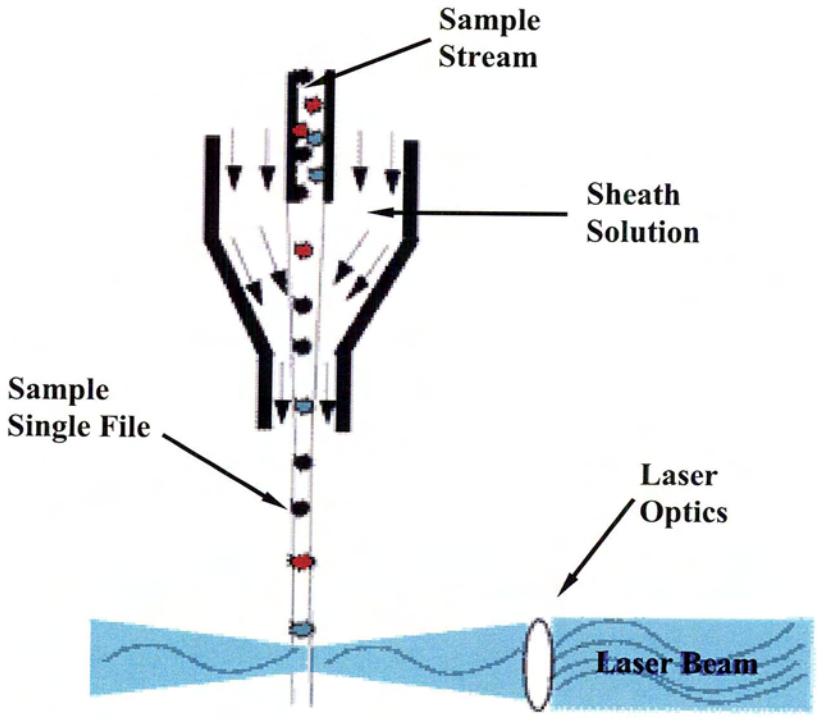

Figure 3.2 A schematic of the essential components of a flow cytometer.

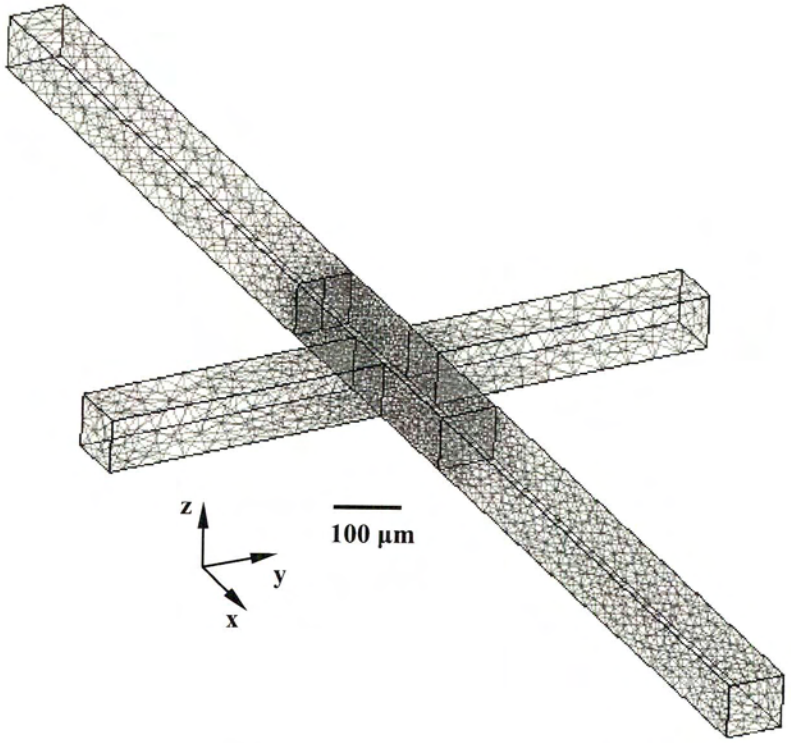

Figure 3.3 Schematic of the microfluidic cross geometry used in the 3-d focusing numerical study. The mesh contains ~20 000 finite elements, refined in regions where high concentration gradients exist.

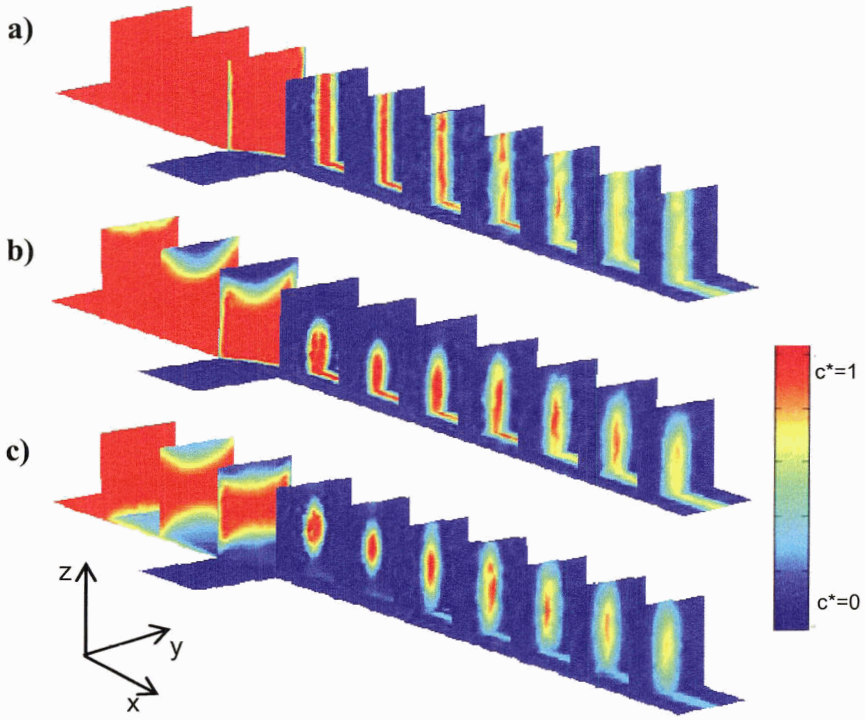

Figure 3.4 Cross-sectional concentration fields are plotted at 100μm intervals along the central channel of three focusing cases: a) homogeneous surface charge distribution, b) surface patch on top surface only, and c) surface patches on top and bottom surfaces.

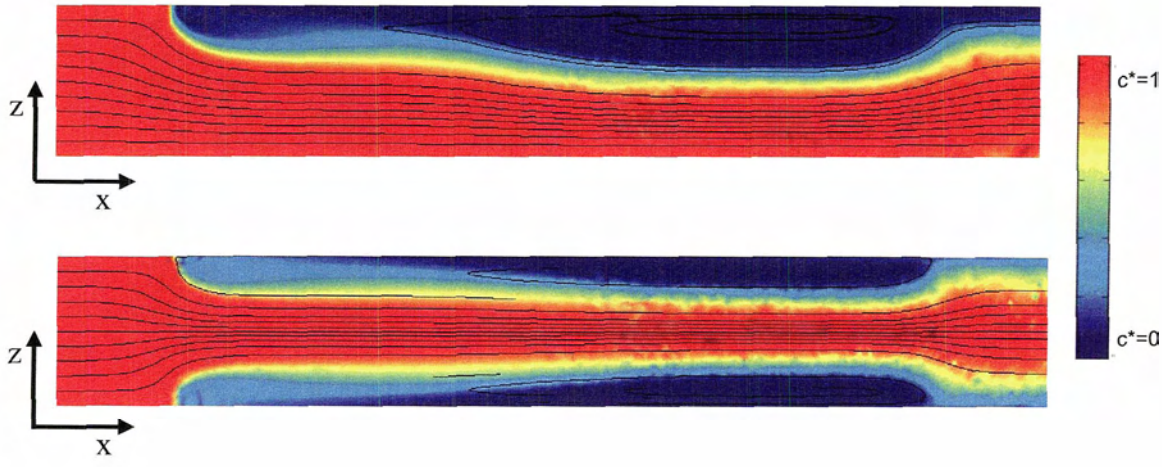

Figure 3.5 Concentration profiles are shown for a cross section taken along the centerline of the main channel for the top surface patch case (a) and the top and bottom surface patch case (b). Streamlines show the three dimensional focusing of the sample stream through evidence of the recirculation zones.

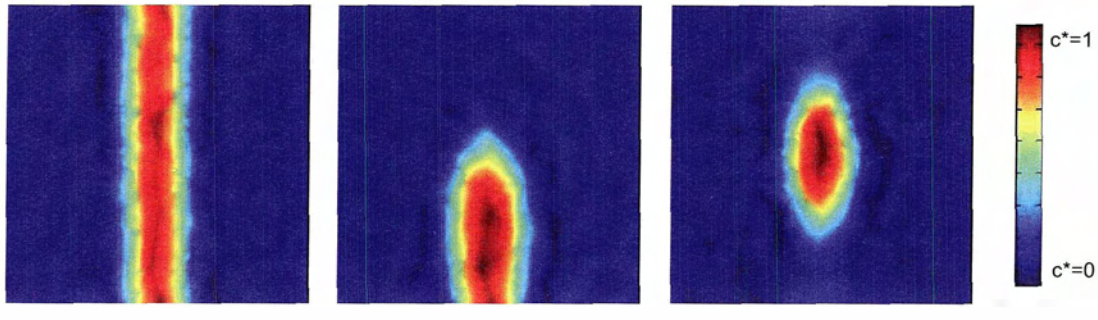

Figure 3.6 Cross-sectional concentration fields are plotted for the three focusing cases at a point 200μm downstream of the intersection. The sample stream area is reduced to 17%, 13%, and 12% for the homogeneous, top, and top and bottom surface charge cases respectively.

Chapter 4

CONCLUSIONS AND FUTURE WORK

4.1 Conclusions and Contributions of this Thesis

This thesis was devoted to the development of electrokinetic processes which extend the capabilities of microfluidic devices. The contributions of this work include the development of a numerical model to study electroosmotic microflows, the design and development of a novel microfluidic mixing strategy, the experimental validation of the micromixer performance, and the development of a novel three-dimensional hydrodynamic focusing strategy. The development of the experimental facilities in the UVic Microfluidics Lab was an additional contribution of this thesis work. The key contributions are summarized below.

4.1.1 High Efficiency Microfluidic Mixing through Symmetric Sample Injection

A novel microfluidic mixing strategy is developed which exploits stream-wise diffusive mixing of a sequence of injected samples in an electroosmotic flow. Numerical simulations demonstrate the method and predict its performance. Sequential injection micromixing is first considered using ideal concentration inputs to optimize the geometry

and switch frequency. To facilitate sequential injection on-chip, new sequential injection schemes are developed and coupled with an expansion region. Next, an experimental study is performed on the symmetry-based sequential injection microfluidic mixer. Fluorescence microscopy is employed to analyze, quantify and demonstrate the effectiveness of this mixing strategy, as well as to determine an optimal frequency range for operation. In addition, it is demonstrated experimentally that that outlet concentration can be actively controlled by adjusting the duty cycle of the applied switch frequency.

4.1.2 Three-Dimensional Hydrodynamic Focusing

A three-dimensional numerical model was applied to demonstrate that steady-state three-dimensional hydrodynamic focusing can be achieved in a planar microfluidic cross geometry using strategically-placed surface charges. Configurations with one and two surface patches were found to achieve a high degree of focusing in the depthwise direction, while maintaining the planar focusing accomplished by the sheath flows. The microfluidic streams were focused to 13% and 12% of their original cross-sectional areas for the cases of one and two surface patches, respectively. The two patch design has the added benefit that the sample stream is focused to the centre of the microchannel and has minimal contact with the microchannel walls in the detection region; an important consideration for some readily adsorbed biological analytes.

4.2 Proposed Extensions of this Work

There are many aspects of this work which have uncovered opportunities for future projects and some of these are discussed below.

4.2.1 Experimental Validation of Three-Dimensional Focusing

The numerical study of the three-dimensional hydrodynamic focuser provided promising results. Currently, this technology is being studied experimentally. The surface charge patterning is obtained using the procedure of Katayama et al. (1998), where an ionic polymer modifies the zeta potential of the surface. The surface charge patches used in the numerical study are ideal, and cannot be easily reproduced on a physical chip. However, we have recently shown that a similar effect can be obtained by treating the sheath-flow channels and adjusting the applied electric fields accordingly. Diffusion of the treatment solution into the sample channel produces the required surface patch. Initial results have shown evidence of the circulation region, however, quantitative results will require the use of a confocal microscope for the necessary depthwise measurements. These measurements are currently underway.

4.2.2 Microfluidic Memory

It was observed during the study of surface patch induced flow circulations that the opportunity exists for short-term partitioning and storage of a sample solution. Consider the case of a single straight channel with an axially-localized cross-sectional surface patch (ring). The surface patch ring surrounds the channel resulting in an annular circulation pattern. If the surface patch is given a surface charge opposite to that of the native surface, flow circulations will be produced under an axially applied electric field.

As the sample stream flows through this region, the fluid will become entrapped in the circulation zone and equilibrate, leaving a uniform concentration field. However, when the new solution is introduced, the front is focused through the centre of the annular circulation, whereas the circulation-entrapped fluid will initially retain its original concentration. The injected solution will gradually diffuse into the circulation-entrapped fluid until a new equilibrium is attained. The entrapped-fluid is expected to have a 'memory' on the order of 2 seconds based on the results of preliminary numerical studies. Establishing the experimental proof-of-concept of this technology is a future project.

4.2.3 Enhanced Pinched Injection

Using the concept of surface patch induced flow circulations, a more uniform sample shape can be produced during a pinched injection. Circulations can be generated on the side walls of a microfluidic cross with surface patches, to pre-focus the sample stream before it enters the dispensing region. The patches are placed along the side walls at the channel cross. Flow will be entrained into the resulting circulations from the sheath buffer solution. Two stage focusing schemes have previously been developed, however this proposed method would involve only a single step. Unfortunately, several aspects limit the applicability of this injector: Firstly, it is not straightforward to vary the degree of focusing as the circulation concentration is highly dependant on field strength. Secondly, the heterogeneous patches have the potential to disturb the pre-focused sample shape during the dispensing step. Lastly, the requirement of 'side-treated' microchannels presents some significant challenges with respect to accurate surface treatment during fabrication.

References

Alarie, J. P, Jacobson, S. C., Ramsey, J. M. (2001) "Electrophoretic Injection Bias in a Microchip Valving Scheme." Electrophoresis, 22, 312-317.

Bianchi, F., Ferrigno, R., Girault, H. H., (2000) "Finite Element Simulation of an Electroosmotic-Driven Flow Division at a T-junction of Microscale Dimensions" Analytical Chemistry, 72:1987-1993

Biddiss, E., Erickson, D., and Li, D. (2004) "Heterogeneous Surface Charge Enhanced Micromixing for Electrokinetic Flows" Analytical Chemistry, 76, 3208 – 3213.

Bird, R., Stewart, W. E, and Lightfoot, E. N. (1960) "Transport Phenomena" John Wiley & Sons, New York, NY.

Bousse, L., Cohen, C., Nikiforov, T., Chow, A., Kopf-Sill, A. R., Dubrow, R., Parce, W. (2000) "Electrokinetically Controlled Microfluidic Analysis Systems" Annual Review of Biophysical and Biomolecular Structures, 29, 155-181.

Breuer, K. S. (ed) (2004) Microscale Diagnostic Techniques, Springer, New York Berlin Heidelberg.

Brody, J.P., Yager, P. Goldstein, R. E., Austin, R. H. (1996) "Biotechnology at Low Reynolds Numbers" Biophysical Journal, 71, 3430-3441.

Chou, H-P., Spence, C., Scherer, A., and Quake, S. (1999) "A Microfabricated Device for Sizing and Sorting DNA Molecules" Applied Physical Sciences, Biophysics, 96, 11 – 13.

Coleman, J. T. and Sinton, D. (2005a) "A Sequential-Injection Microfluidic Mixing Strategy" Journal of Microfluidics and Nanofluidics, Available Online.

Coleman, J. T., McKechnie, J., and Sinton, D. (2005b – Submitted) "High Efficiency Electrokinetic Micromixing through Symmetric Sequential Injection" Analytical Chemistry.

Coleman, J. T., McKechnie, J., and Sinton, D. (2005c) "A Symmetry-Based Microfluidic Mixer for Rapid and Complete Mixing" International Conference on Microchannels and Minichannels, Toronto, Canada, June 13 – 15.

Coleman J. T., Lansdorp, B., and Sinton, D. (2005d) "Three-Dimensional Microfluidic Focusing with Surface Charge Patterning" International Conference on Microchannels and Minichannels, Toronto, Canada, June 13 – 15.

Coleman, J. T., and Sinton, D. (2004) "Microfluidic Mixing Through Sequential Sample Injection with Rapid Expansion" International Mechanical Engineering Congress and RD&D Exposition, Anaheim, CA, USA, Nov. 13 – 19.

Culbertson, C. T., Jacobson, S. C., and Ramsey, J. M. (1998) "Dispersion Sources for Compact Geometries on Microchips" Analytical Chemistry, 70, 3781 – 3789.

Deshmukh, A. A., Liepmann. D., and Pisano, A. P. (2000) "Continuous Micromixer with Pulsatile Micropumps" Proceedings of IEEE Solid-State Sensor and Actuator Workshop, SC, USA, pp. 779-782.

Duffy, D. C., McDonald, J. C., Schueller, O. J. A., Whitesides, G. M. (1998) "Rapid Prototyping of Microfluidic Systems in Poly(dimethylsiloxane)." Analytical Chemistry, 70, 4974-4984.

Erickson, D., and Li, D., (2003a) "Three-Dimensional Structure of Electroosmotic Flows over Heterogeneous Surfaces" Journal of Physical Chemistry B, 107, 12212-12220.

Erickson, D., Sinton, D., Li, D. (2003b) "Joule Heating and Heat Transfer in Poly(dimethylsiloxane) Microfluidic Systems." Lab on a Chip, 3, 141-149.

Erickson, D., and Li, D. (2002) "Influence of Surface Heterogeneity on Electrokinetically Driven Microfluidic Mixing." Langmuir, 18, 1883-1892.

Ermakov, S. V., Jacobson, S. C., Ramsey, J. M. (1998) "Computer Simulations of Electrokinetic Transport in Microfabricated Channel Structures." Analytical Chemistry, 70, 4494-4504.

Ermakov, S. V., Jacobson, S. C., Ramsey, J. M. (2000) "Computer Simulations of Electrokinetic Injection Techniques in Microfluidic Devices." Analytical Chemistry, 72, 3512-3517.

Fu, A., Spence, C., Scherer, A., Arnold, F.H., and Quake, A.R. (1999) "A Microfabricated Fluorescence-Activated Cell Sorter" Nature Biotechnology, 17, 1109 – 1111.

Fujii, T., Sando, Y., Higashino, K, and Fujii, Y. (2003) "A Plug and Play Microfluidic Device" Lab on a Chip, 3, 193 – 197.

Glasgow, I. and Aubry, N. (2003) "Enhancement of Microfluidic Mixing Using Time Pulsing", Lab on a Chip, 3, 114 – 120.

Glasgow, I., Lieber, S., and Aubry, N. (2004a) "Parameters Influencing Pulsed Flow Mixing in Microchannels" Analytical Chemistry, 76, 4825 – 4832.

Glasgow, I., Batton, J., and Aubry, N., (2004b) "Electroosmotic Mixing in Microchannels" Lab on a Chip, 4, 558 – 562.

Goranovic, G., Perch-Nielson, I.R., Larsen, U. D., Wolff, A., Kutter, J. P., and Telleman, P. (2001) "Three-Dimensional Single Step Flow Sheathing in Micro Cell Sorters" Modeling and Simulation of Microsystems.

Hertzog, D. E, Michalet, X., Jager, M., Kong, X., Santiago, J.G., Weiss, S., and Bakajin, O. (2004) "Femtomole Mixer for Microsecond Kinetic Studies of Protein Folding" Analytical Chemistry, 76, 7169 – 7178.

Haugland, R. P. (1994) "Spectra of Fluorescent Dyes Used in Flow Cytometry," Methods in Cellular Biology, 42, 641–663.

Hunter, R. J. (1981) "Zeta Potential in Colloid Science: Principles and Applications" Academic Press, New York, NY.

Inoue, S., and Spring, K. R., (1997) Video Microscopy the Fundamentals, 2nd Ed., Plenum Press, New York, NY.

Jacobson, S. C., Culbertson, C. T., Daler, J. E., Ramsey, J. M. (1998) "Microchip Structures for Submillisecond Electrophoresis." Analytical Chemistry, 70, 3476-3480.

Jacobson, S. C., McKnight, T. E., and Ramsey, J. M, (1999) "Microfluidic Devices for Electrokinetically Driven Parallel and Serial Mixing" Analytical Chemistry, 71, 4455-4459.

Jahn, A., Vreeland, W. N., Gaitan, M., and Locascio, L. E. (2004) "Controlled Vesicle Self-Assembly in Microfluidic Channels with Hydrodynamic Focusing" Journal of American Chemical Society, (Communication), 126(9), 2674-2675.

Jeon, N. L., Dertinger, K. W, Chiu, D. T., Choi, I. S., Stroock, A. D., Whitesides, G. M. (2000) "Generation of Solution and Surface Gradients Using Microfluidic Systems" Langmuir, 16, 8311- 8316.

Johnson, T. J., Ross, D., and Locascio, L. E. (2002) "Rapid Microfluidic Mixing" Analytical Chemistry, 74, 45-51.

Kamholz, A. E., (2004) "Proliferation of Microfluidics in Literature and Intellectual Property" Lab on a Chip, 4, 16N–20N

Katayama, H., Ishihama, Y., and Asakawa, N. (1998a) "Stable Capillary Coating with Successive Multiple Ionic Layers" Analytical Chemistry, 70, 2254 – 2260.

Katayama, H., Ishihama, Y., and Asakawa, N. (1998b) "Stable Cationic Capillary Coating with Successive Multiple Ionic Polymer Layers for Capillary Electrophoresis" Analytical Chemistry, 70, 5272 – 5277.

Kirby, B. J. and Hasselbrink, E. F. (2004a) "Zeta Potential of Microfluidic Substrates: 1. Theory, Experimental Techniques, and Effects on Separations" Electrophoresis, 25, 187 – 202.

Kirby, B. J. and Hasselbrink, E. F. (2004b) "Zeta Potential of Microfluidic Substrates: 2. Data for Polymers" Electrophoresis, 25, 203 - 213.

Li, D. (2004) Electrokinetics in Microfluidics, Academic Press, New York.

Lin, C-H., Fu, L. M., and Chien, Y. S. (2004a) "Microfluidic T-Form Mixer Utilizing Switching Electroosmotic Flow" Analytical Chemistry, 76, 5265 – 5272.

Lin, C-H., Lee, G-B., Fu, L-M., and Hewy, B. H. (2004b) "Vertical Focusing Device Utilizing Dielectrophoretic Force and Its Application on Microflow Cytometer" Journal of Microelectromechanical Systems, 13, 923 – 932.

Lin, C-H, and Lee, G-B. (2003) "Micromachined Flow Cytometers with Embedded Etched Optic Fibers for Optical Detection" Journal of Micromechanics and Microengineering, 13, 447 – 453.

Liu, R. H., Stremler, M. A., Sharp, K. V., Olsen, M. G., Santiago, J. G., Adrian, R. J., Aref, H., and Beebe, D. J. (2000) "Passive Mixing in a Three-Dimensional Serpentine Microchannel" Journal of Microelectromechanical Systems, 9, 190-197.

Liu, Y., Fanguy, J. C., Bledsoe, J. M., and Henry, C. S. (2000) "Dynamic Coating Using Polyelectrolyte Multilayers for Chemical Control of Electroosmotic Flow in Capillary Electrophoresis Microchips" Analytical Chemistry, 72, 5939 – 5944.

McDonald, J. C., Duffy, D. C., Anderson, J. R., Chiu, D. T., Wu, H., Schueller, O. J. A., and Whitesides, G. M. (2000) "Fabrication of Microfluidic Systems in Poly(dimethylsiloxane)" Electrophoresis, 21, 27-40.

Nguyen, N-T, and Wereley, S. T. (2002) "Fundamentals and Applications of Microfluidics" Artech House, Norwood, MA

Nguyen, N-T. and Wu, Z. (2005) "Micromixers – A Review" Journal of Micromechanical Microengineering, 15, R1 – R16.

Oddy, M. H., Santiago, J. G., and Mikkelsen, J. C. (2001) "Electrokinetic Instability Micromixing" Analytical Chemistry, 73, 5822-5832.

Patankar, N. A., and Hu, H. H. (1998) "Numerical Simulation of Electroosmotic Flow." Analytical Chemistry, 70, 1870-1881.

Santiago, J. G. (2001) "Electroosmotic Flows in Microchannels with Finite Inertial and Pressure Forces." Analytical Chemistry, 73, 2352-2365.

Schrum, D. P., Culbertson, C. T., Jacobson, S. C., and Ramsey, J. M. (1999) "Microchip Flow Cytometry Using Electrokinetic Focusing" Analytical Chemistry, 71, 4173 – 4177.

Sharp, K. V., Adrian, R. J., Santiago, J. G., and Molho, J. I. (2002) "Liquid Flows in Microchannels" In: Gad-el-Hak M (ed), CRC Handbook of MEMS. CRC Press, New York, pp. 6-1–6-38.

Shapiro, H. M. (2003) Practical Flow Cytometry, 4th Ed., Wiley-Liss

Sinton, D., (2004) "Microscale Flow Visualization." Journal of Microfluidics and Nanofluidics, 1, 2-21.

Sinton, D., Ren, L., and Li, D. (2003a) "A Dynamic Loading Method for Controlling On-Chip Microfluidic Sample Injection" Journal of Colloid and Interface Science, 266, 448-456.

Sinton D, Ren L, Xuan X, Li D (2003b) "Effects of Liquid Conductivity Differences on Multi-Component Sample Injection, Pumping and Stacking in Microfluidic Chips" Lab on a Chip, 3, 173–179.

Stone, H. A., Kim, S. (2001) "Microfluidics: Basic Issues, Applications and Challenges" American Institute of Chemical Engineers Journal, 47:1250–1254.

Stone, H. A., Stroock, A. D., and Ajdari, A., (2004) "Engineering Flows in Small Devices: Microfluidics Toward a Lab-on-a-Chip" Annual Revue of Fluid Mechanics 36:381–411.

Stroock, A. D., Dertinger, S. K. W., Ajdari, A., Mezić, I., Stone, H. A., and Whitesides, G. M. (2002) "Chaotic Mixer for Microchannels" Science, 295, 647-651.

Sundararajan, N., Pio, M. S., Lee, L. P., and Berlin, A. A. (2004) "Three-Dimensional Hydrodynamic Focusing in Polydimethylsiloxane (PDMS) Microchannels" Journal of Microelectromechanical Systems, 13, 559 – 567.

Tang, Z., Hong., S., Djukic, D., Modi, V., West, A.C., Yardley, J., and Osgood, R.M., 2002, "Electrokinetic Flow Control for Composition Modulation in a Microchannel" Journal of Micromechanics Microengineering, 12, 870 – 877.

Weaver, J. L. (2000) "Introduction to Flow Cytometry" Methods, 21, 199–201.

White, F. M., 1974, Viscous Fluid Flow, McGraw-Hill, New York, NY.

Whitesides, G. M., and Stroock, A. D., (2001) "Flexible Methods for Microfluidics" Physics Today 54(6):42–48

Yang, R., Feeback, D. L., and Wang, W. (2005) "Microfabrication and Test of a Three-Dimensional Polymer Hydro-Focusing Unit for Flow Cytometry Applications" Sensors and Actuators A, 118, 259 – 267.